



# Numerical investigation of evaporative cooling strategies on the aero-thermal performance of courtyard buildings in hot-dry climates

Hao Sun<sup>a,\*</sup>, Hua Zhong<sup>b,c</sup>, Abdullah Dik<sup>a,d</sup>, Kemin Ding<sup>a</sup>, Carlos Jimenez-Bescos<sup>e,f</sup>, John Kaiser Calautit<sup>a</sup>

<sup>a</sup> Department of Architecture and Built Environment, University of Nottingham, UK

<sup>b</sup> School of Built Environment and Architecture, London South Bank University, UK

<sup>c</sup> School of Architecture, Design and Built Environment, Nottingham Trent University, UK

<sup>d</sup> Faculty of Engineering, Iskenderun Technical University, Hatay, Turkey

<sup>e</sup> Westminster Business School, University of Westminster, UK

<sup>f</sup> School of Built and Natural Environment, University of Derby, UK

## ARTICLE INFO

### Keywords:

Aero-thermal performance  
CFD modelling  
Single-sided ventilated courtyard  
Cross-ventilated courtyard  
Water sprayer  
Evaporative cooling strategy

## ABSTRACT

In hot and dry urban environments, courtyards help mitigate extreme heat and influence the urban microclimate. These structures not only provide light and private outdoor spaces but also aid in mitigating the urban heat island (UHI) effect through improved airflow and evapotranspiration. Courtyards, being central open-air areas enclosed by buildings, are crucial in creating opportunities for natural ventilation driven by wind and buoyancy-induced forces, thus serving as a microclimatic regulator. This study investigates the role of courtyards in modulating their microclimate and adjacent indoor areas by integrating evaporative cooling strategies to enhance cooling in these spaces. While numerous studies have been conducted on the role of water bodies in evaporative cooling, the aero-thermal impact on adjacent indoor spaces remains less understood. Addressing this gap, the present research explores the effect of an evaporative cooling system on the wind and thermal conditions within a courtyard and examines different natural ventilation modes, namely, single-sided and crossflow ventilation, in indoor spaces. A computational fluid dynamics (CFD) model, validated against wind tunnel experimental data, was employed to simulate various evaporative cooling water spray configurations. The results reveal complex courtyard microclimates with diverse cooling effects influenced by room orientation and floor level. Specifically, in single-sided ventilated courtyards, water sprays significantly improved the indoor thermal environment, with the average temperature across all rooms decreased by 2.06 °C, and humidity increased by 4.29 %. However, in cross-ventilated courtyards, water sprays' cooling and humidifying effects were relatively less effective. This research underscores the potential of evaporative cooling technology in improving the microclimate of courtyards, with practical applications extending to urban design and architecture. By tailoring cooling strategies to specific courtyard configurations, urban planners and architects significantly improve indoor comfort levels and energy efficiency.

## 1. Introduction and literature review

### 1.1. Background and motivation

The increase in extreme weather events, coupled with the urban heat island (UHI) phenomenon, has amplified concerns about global warming and climate change. Many societies recognize these issues as top priorities [1]. One of the most detrimental consequences of climate change on buildings is overheating, particularly pronounced in hot and

dry climate regions [2]. Studies have indicated that such conditions significantly exacerbate the overheating of building interiors. This not only affects the comfort and health of occupants but also increases the energy consumption of active cooling systems, exacerbating energy crises and environmental pollution issues [3,4]. Additionally, the UHI phenomenon has significantly contributed to the exacerbated overheating in cities. Predictions suggest that the rise in global average temperatures will lead to increasingly frequent and prolonged heat-waves. However, relying solely on expanding active cooling systems is

\* Corresponding author. Department of Architecture and Built Environment, University of Nottingham, UK.

E-mail addresses: [Hao.Sun@nottingham.ac.uk](mailto:Hao.Sun@nottingham.ac.uk) (H. Sun), [John.Calautit1@nottingham.ac.uk](mailto:John.Calautit1@nottingham.ac.uk) (J.K. Calautit).

<https://doi.org/10.1016/j.buildenv.2024.111588>

Received 12 December 2023; Received in revised form 20 March 2024; Accepted 27 April 2024

Available online 1 May 2024

0360-1323/© 2024 The Authors. Published by Elsevier Ltd. This is an open access article under the CC BY license (<http://creativecommons.org/licenses/by/4.0/>).

not an appropriate solution, especially given the current energy landscape and the fact that resources have not been fully optimized. The growing energy consumption of buildings substantially burdens the energy sector [5]. Studies have shown that over 40 % of global energy consumption comes from buildings and is continuously growing [6]. As a result of an increase in the frequency and intensity of overheating, cooling energy consumption in summer is anticipated to rise by 72 % globally by 2100 [7]. Passive cooling methods can improve energy efficiency, reduce interior overheating, and improve thermal comfort [8]. However, it is crucial to correctly select and implement passive cooling technology to improve the energy efficiency of buildings [9].

## 1.2. Literature review

The courtyard is a passive cooling strategy and one of the most common architectural features in the design of traditional buildings. Wind-driven forces and the temperature differential between the courtyard and the inside spaces drive the natural ventilation flows. Internal courtyards have been shown to enhance the effectiveness of natural ventilation, which could reduce overheating within the building [10]. On the warmest day of the year in the Netherlands, Taleghani et al. monitored the air temperature to investigate three different architectural forms: courtyards, pavilions, and conventional structures. It was found that the courtyard offers the most favourable microclimate conditions among the three urban types. In order to identify the optimal courtyard building form, Al-Masri and Abu-Higleh [11] conducted energy simulations of courtyard buildings. The authors demonstrated that the basic courtyard construction model with the original building materials decreased annual energy usage by 6.9 %. The improved courtyard model decreased by 11.2 % annual energy consumption, as compared with other building forms. Several studies employed numerical models and field measurement techniques to examine the impacts of courtyard design, including geometry, proportions, orientation, and materials, on thermal conditions, ventilation, and energy consumption of courtyard buildings [12]. Rojas et al. [13] compared numerical findings from CFD to air temperature measurements between the semi-enclosed courtyard and the enclosed courtyard of a hotel in Spain, with a noticeable difference in the flow pattern observed. Ernest et al. [14] examined several courtyard designs to establish convective cooling functions in transitional areas. They reported that the orientation of the courtyard impacts the thermal and energy efficiency of the surrounding buildings. However, it's important to note that while these studies provide valuable insights into the passive strategies of courtyards, they may not fully encompass the variability of factors in different scenarios, including the application of other passive methods in courtyard architectures and exploration in various climate conditions.

Some courtyards are integrated with trees, flowers, water ponds and fountains, creating a tranquil and visually appealing environment. Additionally, these features provide shade and regulate the microclimate by increasing relative humidity [9,15]. In many contexts, evaporative cooling systems are favoured over introducing vegetation within courtyards. Typically, water bodies exhibit a more pronounced cooling effect than vegetation, although this can vary based on location and climatic conditions [16]. Water bodies, such as ponds, pools, or fountains, are effective in reducing the ambient temperature of interior courtyards and their surrounding regions [17]. In hot and dry areas, evaporation lowers the air temperature and humidifies the air. In an enclosed space such as a central courtyard, the extent of evaporation depends on the surface area of the water, the relative humidity of the air and the temperature of the water [18].

Evaporative cooling through a water sprayer system is an efficient method for relieving overheating and enhancing thermal comfort indoors and outdoors, especially in hot and dry climates [19]. Traditional techniques, such as planting plants and enhancing shortwave reflectance, typically have year-round effects that are difficult to regulate. While they can provide a positive impact during the warmer months,

they can lead to increased building energy consumption in winter [20]. Assessing the efficacy of water sprayer systems has been challenging, leading most studies to rely on field measurements. To evaluate the performance of water sprayer systems, various physical characteristics were analyzed for their influence. Sureshkumar et al. [19] investigated the cooling effect of a water spray system with hollow cone nozzles using different nozzle sizes and different water flow rates. Conducting field experiments to obtain accurate measurements can be daunting due to uncontrollable parameters such as wind speed and direction. However, CFD simulation can provide a viable solution by facilitating simulations with various set parameters. Additionally, CFD simulation allows for modelling two-phase flows in spray systems. Montazeri et al. [21,22] assessed the evaporative cooling impact of droplets in two-phase flows using a validated CFD model and analyzed the effect of various parameters on the cooling performance. Moreover, Zhong et al. [23,24] conducted numerical simulations of the cooling effect of water spray systems in a stadium and a greenhouse. Montazeri et al. [20] evaluated the cooling effect of a water spray system with 15 hollow-cone nozzles in a courtyard, comparing it to a scenario without the spray system. The results indicated that when the water flow rate was 9.0 l/min and the system was positioned at a height of 3 m, the most significant temperature reduction (about 7 °C) occurred under the spray system. Additionally, they studied the effects of varying water flow rates (2.25, 4.50, 9.0 l/min) and different heights of the water spray system. The study found that higher water flow rates resulted in a broader coverage of the cooling effect. When the height of the water spray system was increased from 3 m to 5 m, the maximum air temperature decreased by approximately 2 °C [20]. Their research primarily focused on the direct cooling effects within the courtyard, while an in-depth exploration of how such cooling strategies affect the temperature and humidity conditions of adjacent indoor spaces has not yet been conducted.

## 1.3. Research gaps and novelty

Previous research on the thermal and wind environment in courtyard buildings has primarily concentrated on the courtyards themselves, including aspects such as geometry and orientation, with limited exploration into the integration of passive technologies like evaporative cooling systems within the courtyards. Furthermore, while the cooling effects of water sprayers in courtyards have been acknowledged, their impact on the indoor thermal and wind environments of surrounding buildings has been scarcely investigated. This oversight extends to a detailed examination of how different ventilation strategies, specifically single-sided versus crossflow ventilation, influence these indoor conditions.

This study addresses research gaps by analyzing the impact of evaporative cooling systems in courtyard buildings, an area not extensively studied before. It investigates the impact of these systems on both the courtyards themselves and the indoor environments of surrounding buildings. Additionally, it examines the role of courtyard architectural features, such as different ventilation strategies, in improving indoor aero-thermal conditions. These strategies include cross ventilation (openings on multiple facades) and single-sided ventilation (openings on only one facade [25,26]). The novelty of this research lies in its examination of how evaporative cooling strategies, combined with specific architectural configurations of courtyard buildings, can improve the microclimate in both outdoor and indoor environments of courtyard buildings. This focus on the interaction between outdoor and indoor spaces and the analysis of ventilation strategies contributes insights for designing urban dwellings that are more comfortable and energy-efficient in hot-dry climates.

## 1.4. Aim and objectives

This study examines the wind and thermal performance of courtyard buildings integrated with natural ventilation techniques and water

sprayer systems, using ANSYS Fluent for CFD modelling. It specifically investigates the impact of water sprayers on the aero-thermal conditions around courtyards in a hot and dry region to determine the suitability of cross and single-sided ventilation strategies in courtyard buildings when combined with evaporative systems. The study will validate the CFD simulation results against wind tunnel experimental data. The evaluation will consider factors such as wind speed, air temperature, and relative humidity in various courtyard building locations. It is worth noting that our study has some limitations. Firstly, there is a certain degree of error between wind tunnel experiments and CFD simulations, and due to the complexity of the model and the influence of external environmental factors, errors are inevitable. Secondly, this study did not involve on-site experiments but conducted CFD simulations based on a simplified version of the wind tunnel model. The limitation of this method lies in the possibility of not being able to fully capture the various complex factors in the real environment.

In the sections that follow, Section 2 details the methodologies, including CFD approaches that cover the development of models, numerical methods, mesh analysis, and settings for boundary conditions. Section 3 presents the study's results, while Section 4 investigates the aero-thermal performance of each room under varying water flow rates and discusses the limitations of this study. Finally, Section 5 offers a conclusion and outlines directions for potential future research.

## 2. Method

In the methodology section, we initiated our exploration with an analysis of the theoretical foundations of CFD and the definition of the solver settings. Subsequently, we described the courtyard model, including its dimensions, structural layout, and configuration in the simulation environment. Next, we presented the fluid domain setup, including the determination of the spatial range and key characteristics of fluid flow. These chosen settings ensured the simulation environment's accurate capture of key phenomena in fluid dynamics. Additionally, we showcased specific details of the grid design, including the type, size, and distribution strategy of the grid, aimed at capturing complex phenomena. The accuracy and stability of the simulation results were assessed through mesh independence verification. Finally, this section explains the simulation's boundary conditions, including fluid inlet and outlet conditions, wall conditions, and other boundary conditions.

### 2.1. CFD theory

The steady-state, three-dimensional simulations were performed using the ANSYS Fluent 2021R2 CFD tool and the Reynolds-Averaged Navier-Stokes (RANS) equations. The  $k$ -epsilon Realizable model [27] was utilized to simulate turbulence, with both continuous and discrete phases of the flow being solved on a fully coupled technique. The following sections will detail the justification for selecting this particular turbulence model. Additionally, the droplet momentum, heat, and mass transport equations are addressed in a fully coupled manner within the discrete phase. SIMPLE algorithm is used for pressure-velocity coupling. Second-order interpolation is applied for pressure calculations, and both convective and viscous elements within the equations are solved by a second-order discrete technique. The governing equations, as defined by the commercial CFD code ANSYS/Fluent [28], are as follows:

Continuity Equation:

$$\frac{\partial \rho}{\partial t} + \nabla \cdot (\rho \vec{u}) = 0 \quad (1)$$

Where  $\rho$  is the density,  $t$  is time, and  $\vec{u}$  is the velocity vector.

Momentum Equation:

$$\frac{\partial (\rho \vec{u})}{\partial t} + \nabla \cdot (\rho \vec{u} \vec{u}) = -\nabla p + \nabla \cdot \tau + \rho \vec{g} \quad (2)$$

Where  $p$  is pressure,  $\tau$  is the stress tensor, and  $\vec{g}$  is the gravitational acceleration vector.

Energy Equation:

$$\frac{\partial (\rho E)}{\partial t} + \nabla \cdot (\vec{u} (\rho E + p)) = \nabla \cdot (\kappa_{\text{eff}} \nabla T) + S_h \quad (3)$$

Where  $E$  is the total energy,  $\kappa_{\text{eff}}$  is the effective thermal conductivity,  $T$  is temperature, and  $S_h$  is the heat source term.

The  $k$ -epsilon realizable turbulence model is a semi-empirical model based on model transport equations for the turbulence kinetic energy ( $k$ ) and its dissipation rate ( $\epsilon$ ).

$k$  Equation (Turbulent kinetic energy):

$$\frac{\partial (\rho k)}{\partial t} + \nabla \cdot (\rho \vec{u} k) = \nabla \cdot \left[ \left( \mu + \frac{\mu_t}{\sigma_k} \right) \nabla k \right] + P_k - \rho \epsilon \quad (4)$$

$\epsilon$  Equation (Turbulent dissipation rate):

$$\frac{\partial (\rho \epsilon)}{\partial t} + \nabla \cdot (\rho \vec{u} \epsilon) = \nabla \cdot \left[ \left( \mu + \frac{\mu_t}{\sigma_\epsilon} \right) \nabla \epsilon \right] + C_{1\epsilon} \frac{\epsilon}{k} P_k - C_{2\epsilon} \rho \frac{\epsilon^2}{k} \quad (5)$$

Where  $\mu$  is molecular viscosity,  $\mu_t$  is turbulent viscosity,  $\sigma_k$  and  $\sigma_\epsilon$  are Prandtl numbers,  $C_{1\epsilon}$  and  $C_{2\epsilon}$  are constants, which are 1.44 and 1.9. And  $P_k$  is the production of turbulent kinetic energy.

Species Transport Equation:

$$\frac{\partial (\rho Y_i)}{\partial t} + \nabla \cdot (\rho \vec{u} Y_i) = -\nabla \cdot J_i + R_i \quad (6)$$

Where  $Y_i$  is the mass fraction of the species  $i$ ,  $J_i$  is the diffusion flux, and  $R_i$  is the rate of reaction.

The Discrete Phase Model (DPM) is particularly pertinent for this study involving water sprayers, as it enables a detailed analysis of droplet dynamics. This model is essential for accurately simulating the behaviour of water droplets, including their dispersion, evaporation, and interaction with the surrounding air, which are critical factors in evaluating the effectiveness of the sprayers in modifying the courtyard's microclimate. Eq. (7) to Eq. (10) [22] shows the DPM equations used in this research.

Droplet Motion Equation:

$$\frac{d\vec{U}_d}{dt} = \vec{F}_{\text{drag}} + \vec{F}_{\text{gravity}} + \vec{F}_{\text{buoyancy}} + \vec{F}_{\text{Saffman}} + \vec{F}_{\text{Magnus}} \quad (7)$$

Where  $\vec{U}_d$  is the droplet velocity, and  $\vec{F}_{\text{drag}}$ ,  $\vec{F}_{\text{gravity}}$ ,  $\vec{F}_{\text{buoyancy}}$ ,  $\vec{F}_{\text{Saffman}}$ ,  $\vec{F}_{\text{Magnus}}$  represent forces due to drag, gravity, buoyancy, saffman, and magnus effects, respectively.

Droplet Evaporation and Heat Exchange Equation:

$$\frac{dm}{dt} = -A_d \sum N_i \quad (8)$$

Where  $m$  is the mass of the droplet,  $A_d$  is the surface area of the droplet, and  $N_i$  is the mass transfer rate of species  $i$ .

Mass Transfer Rate Equation:

$$N_i = k_c (C_{i,s} - C_{i,\infty}) \quad (9)$$

Where  $k_c$  is the mass transfer coefficient,  $C_{i,s}$  is the concentration of species  $i$  at the droplet surface, and  $C_{i,\infty}$  is the concentration in the free stream.

Sherwood Number Equation:

$$\text{Sh} = \frac{k_c d_p}{D_{i,m}} = 2.0 + 0.6 \text{Re}_d^{0.5} S_c^{0.33} \quad (10)$$

Sh is the Sherwood number,  $d_p$  is the droplet diameter,  $D_{i,m}$  is the molecular diffusivity of species  $i$ ,  $\text{Re}_d$  is the droplet Reynolds number [22], and  $S_c = 0.7$  is the Schmidt number.

## 2.2. CFD geometry

### 2.2.1. Courtyard and computational domain

The courtyard building models presented in this work were based on the wind tunnel experiments on scaled courtyards and atriums models carried out by Sharples and Bensalem [29], who monitored airflow and air pressure in the courtyard and atriums exposed to the urban wind flow, evaluating various window-to-wall ratios and wind directions [29]. In this study, we utilized courtyard architectural models featuring two distinct ventilation methods, as derived from previous wind tunnel experiments (as shown in Fig. 1). The courtyard models used in these wind tunnel experiments were scaled down to a ratio of 1:100. However, for our CFD simulations, we scaled up the wind tunnel models to their original, actual sizes. This approach ensured that the simulation results more accurately reflected the real courtyard architectural environment.

For both cross-ventilated (CV) and single-sided ventilated (SSV) courtyards, the full-scale sizes ( $L \times W \times H$ ) were  $33.9 \text{ m} \times 33.9 \text{ m} \times 13 \text{ m}$ , as shown in Fig. 2 (a) and Fig. 2 (b). Each courtyard building consisted of four stories, with each floor measuring 3.25 m in height. As depicted in Fig. 2 (d), the courtyard was situated in the centre of the structure, spanning  $12.62 \text{ m} \times 12.62 \text{ m}$ . In the SSV courtyard, all 32 windows faced the courtyard. In contrast, a specific number of windows were allocated on the facade of the CV courtyard building to simulate cross ventilation. The distribution and size of all windows ( $2 \text{ m} \times 1.047 \text{ m}$ ) were retained and consistent with the previous research [29], presenting an 11.4 % window-to-wall ratio, and the window opening ratio was set to 20 % for a more accurate reproduction of the actual scenario as illustrated in Fig. 2 (c). The exact distribution of rooms was applied to the CV courtyard and the SSV courtyard, with each test room measuring 12.62 m in width and 10.64 m in depth. Each floor included four test rooms positioned in east, west, north, and south. All rooms near the courtyard were separately labelled according to the floor and room orientation to analyze the wind and temperature variables in the different rooms as presented in Fig. 2 (e).

This research simulated indoor and outdoor airflow within a single

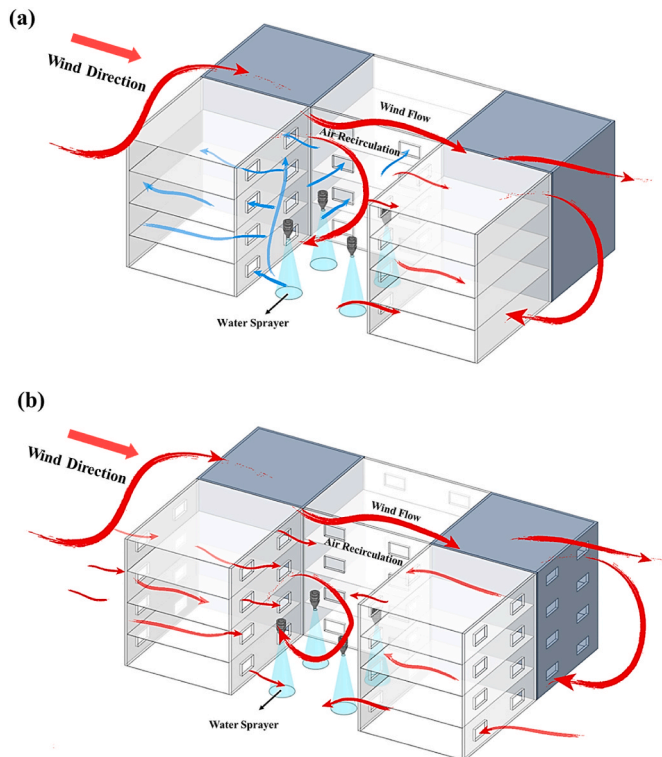


Fig. 1. (a) Single-sided ventilated (SSV) and (b) cross-ventilated (CV) courtyard with water sprayers.

computational domain, as demonstrated in Fig. 3 (a). The domain size generally accords with best practice recommendations for wind flow simulations, as detailed in refs. [30–33]. In the computational domain, both side walls and top wall were defined as symmetry walls. The distances from the courtyard to the two side symmetry walls was set at  $5H$ , where  $H$  is the height of the courtyard building. The distances from the courtyard to the inlet and outlet were set at  $8H$  and  $20H$ , respectively. Additionally, the distance from the courtyard to the top wall of the domain was established at  $5H$ . As can be seen in Fig. 3 (b), in both SSV and CV courtyards, four identical evaporative water sprayers were set, positioned at a height of 6.5 m above the ground and uniformly distributed in the central area of the courtyard. To ensure uniform distances between the injectors, as well as between the injectors and the courtyard walls, the spacing was set at 4.2 m both between each sprayer and from the sprayer to the walls. The water sprayers were directed vertically downward. Detailed boundary conditions are provided in the following sections.

### 2.3. CFD mesh design and verification

The ANSYS 2022 Meshing tool was used to generate the computational domain grid, forming a tetrahedral grid, and the results were imported into Fluent to generate polyhedral meshes, as shown in Fig. 4 (a). In the simulation, to accurately capture the wind-thermal environment within the courtyard and its surrounding buildings, the grid of the entire simulation area was refined to a granularity of 0.2 m. Specifically, for a more precise simulation of the flow characteristics near windows, the grid in these key areas was further refined to a mesh size of 0.05 m. Such grid settings were conducive to capturing flow variations within the indoor environment with greater detail. To reduce the calculation time and to ensure the quality of the mesh, the other areas utilized a coarse grid size of 3.5 m. The mesh settings for both the SSV and CV courtyard were identical.

Sensitivity analysis requires using the same model with different mesh sizes to confirm that the mesh size has a minimal effect on the simulation results. The CV courtyard was selected for grid independence analysis, as detailed in Table 1. In addition to the baseline grid consisting of 1,790,681 cells, classified as a medium-sized grid, two additional grid sizes were generated. A coarse mesh containing 941,223 cells and a fine mesh comprising 6,998,825 cells were generated by adjusting the mesh size for the CV courtyard building.

On the first floor, a horizontal line was drawn, traversing the room and the courtyard. Fig. 4 (b) compares the horizontal wind speed magnitude between five distinct grid sizes. According to the results, the error between the Medium A and the Coarse mesh was 2.65 %, while the error between the Medium A and Fine mesh was 5.12 %. This confirms that the different mesh sizes have minimal impact on the simulation outcomes. Therefore, this study chose the medium A-sized grid to reduce computing power requirements. In subsequent simulation studies, the SSV courtyard model utilized a total of 1,266,979 polyhedral mesh elements (comprising 7,126,317 nodes), while the CV courtyard model employed 1,790,681 polyhedral mesh elements (comprising 9,878,792 nodes).

### 2.4. Boundary conditions for the simulation study

In the setup shown in Fig. 3 (a), a surface was selected as the velocity inlet, and the wind speed distribution at the inlet was determined by referring to atmospheric boundary layer (ABL) wind tunnel experiments to simulate airflow within the computational domain [29]. In all simulated scenarios, the inlet wind speed distribution was maintained consistently. The calculation of the average wind speed was based on a power law formula that was calibrated with wind tunnel measurement data. The formula is defined as follows:

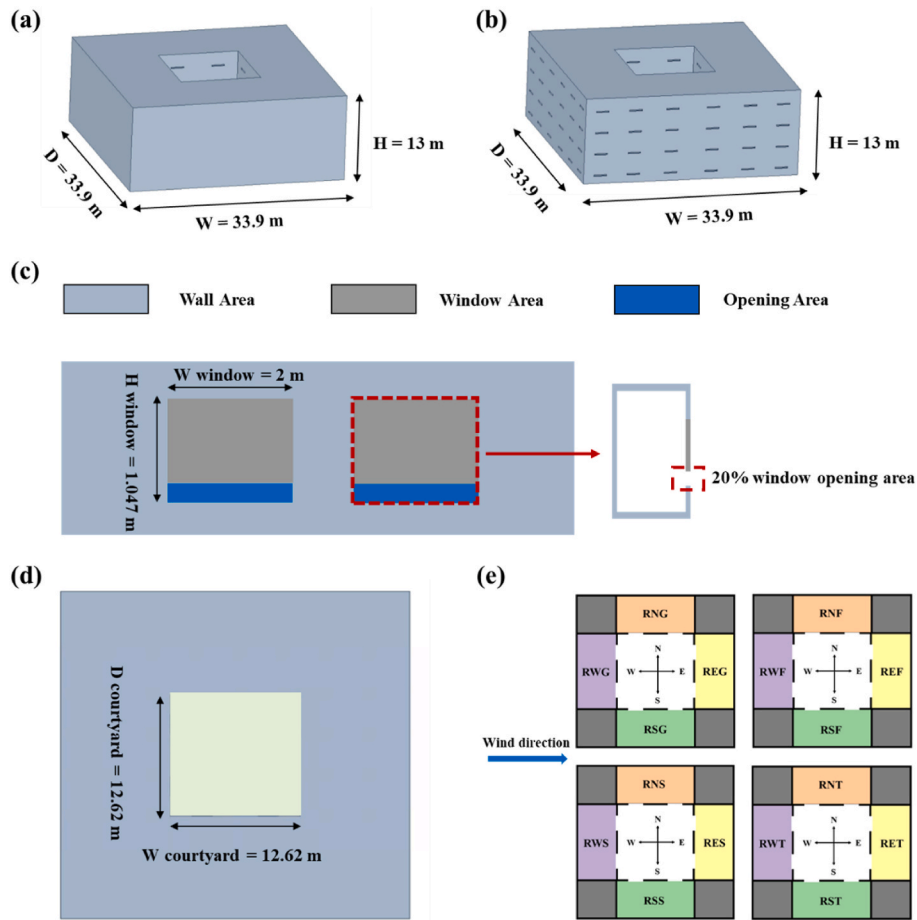


**Fig. 2.** (a) The dimension of the SSV courtyard. (b) The dimension of the CV courtyard. (c) The dimension of each window and the size of the opening area. (d) The location and the size of the courtyard area. (e) The arrangement of each test room (R—Room, N—North, W—West, S—South, E—East, G—Ground floor, F—First floor, S—Second floor, T—Third floor). The second letter on the label represents the orientation and the third represents the floor).

$$u(z) = u_{ref} \left( \frac{z}{z_{ref}} \right)^\alpha \quad (11a)$$

where  $u(z)$  is the mean velocity at height  $z$  (m/s),  $\alpha = 0.245$  is the power law exponent found by curve fitting the wind tunnel result,  $z_{ref} = 800$  mm is the reference height which is the height at the eaves level,  $u_{ref}$  is the velocity measured at the reference height in the experiment, which is 16.4 m/s [29]. Subsequently, this wind speed distribution was applied to the inlet boundary within the computational domain. In this way, the simulation was able to accurately reproduce the wind speed distribution observed in experiments. The opposite side was set as a pressure outlet at 0 Pa.

The study location was based in Seville, Spain (coordinates  $37^\circ 22' 58''$  N,  $5^\circ 58' 23''$  W, elevation 16 m), chosen primarily due to the region's unique climatic conditions and the abundance of traditional courtyard buildings. Particularly during the hot seasons, Seville frequently experiences heatwaves, prompting a thorough analysis of the courtyards' regulatory functions and thermal environment [34,35]. Given the focus of this study on hot and dry climatic conditions, the temperature ( $40^\circ\text{C}$ ) and relative humidity (15 %) of the region on July 17, 2023, at 6 p.m. were chosen as the inlet boundary conditions for the CFD simulation, maintaining these conditions constant [36]. The purpose of this approach was to analyze the cooling and humidifying effects of water spraying devices in the courtyard environment. The simulation in the CFD included the influence of buoyancy, and the gravity was set to  $-9.81\text{ m/s}^2$ . The top and two side walls were defined as non-slip boundary conditions. For the material settings of the model, ash solid and brick

were utilized for the ground and courtyard structure, respectively.

According to previous works, the evaporative cooling spray system, equipped with four injections, was modelled based on the injection model available in Fluent 2022 [20,21]. The settings for the spray and droplet characteristics are detailed in Table 2. The volume flow rate, temperature, and velocity of water spray were set to 3 l/min,  $30^\circ\text{C}$  and 15 m/s, respectively [20]. The number of droplet streams for the spray was defined as 300, and the Rosin-Rammler model [37] was adopted to establish the diameter distribution of droplets in the simulations. According to the settings of the Rosin-Rammler model [21], the minimum and maximum diameters of droplets taken into account in the simulations were  $74\ \mu\text{m}$  and  $518\ \mu\text{m}$ , respectively, with the mean diameter established at  $369\ \mu\text{m}$  and the spread parameter set at 3.67. In addition, the number of diameters per stream assumed to be introduced into the courtyard space was 20. Additionally, the drag coefficients for the drag force exerted on droplets were estimated by the spherical drag law with the assumption that the droplets remain undeformed.

### 3. Results

#### 3.1. Validation of the courtyard model

The present study performed a numerical evaluation of the ventilation in the SSV and CV courtyards. While the earlier studies conducted simulations to validate the SSV courtyard model against wind tunnel tests [6], the current study used CFD modelling to validate the CV courtyard based on the wind tunnel tests in ref. [29] (see Fig. 5). As

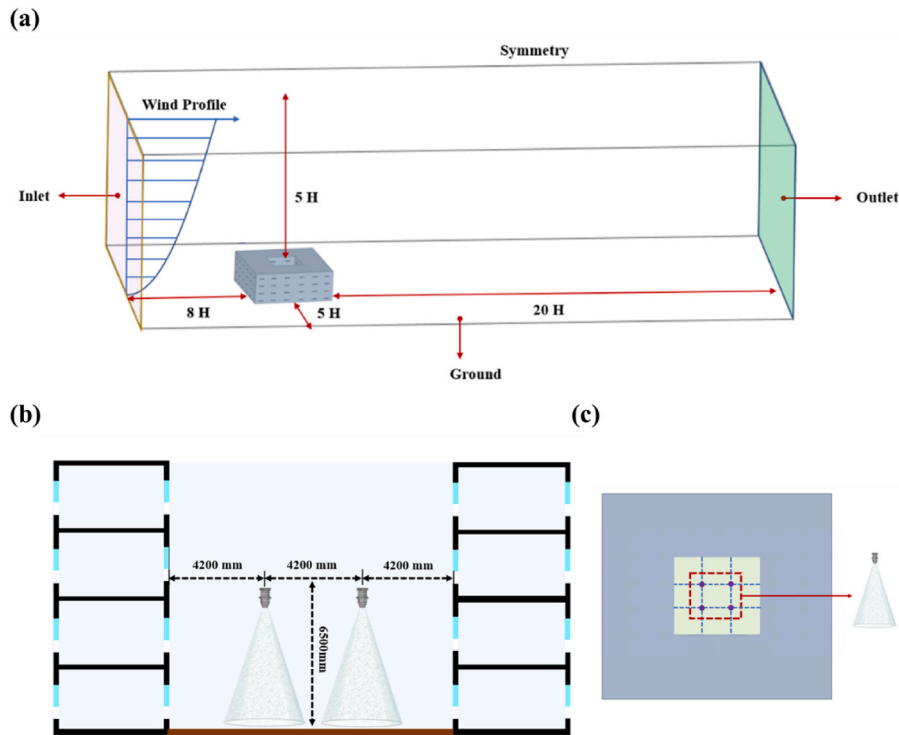


Fig. 3. The simulation setup demonstrating the computational domain and the location of water sprayers. (a) The dimension of the computational domain and the boundary conditions. (b) The dimension and (c) the placement of 4 water sprayers inside the courtyard.

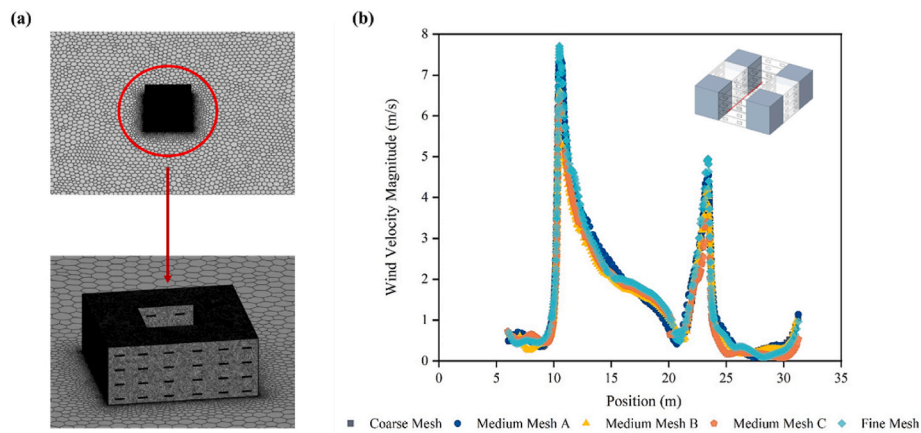


Fig. 4. (a) The courtyard building and outdoor environment surfaces meshed with a polyhedral mesh. (b) Simulated wind speed results along a horizontal centre line of the courtyard model at the height of 4.45 m for the grid sensitivity analysis.

**Table 1**  
Mesh sensitivity analysis for the CV courtyard with polyhedral mesh.

Mesh Size	Mesh Setup		Number of		Average error relative to fine mesh size (%)
	Courtyard building surface size (mm)		Elements	Nodes	
Coarse	300		941,223	4,962,961	7.77
Medium A	200		1,790,681	9,878,792	5.12
Medium B	160		2,793,534	15,517,712	4.16
Medium C	120		5,001,735	28,032,923	3.25
Fine	100		6,998,825	39,334,552	–

detailed in ref. [29], the instrumented model was centrally positioned on a 1.1 m diameter turntable within an ABL wind tunnel. The tunnel has a working length of 7.2 m and a cross-section measuring 1.2 m × 1.2 m,

with the capability to reach a maximum wind speed of 25 m/s.

In their experiments, the airflow in the courtyard and several atrium building models were measured, all sized at 339 mm × 339 mm x 130

**Table 2**  
Summary of the CFD model boundary conditions.

Time	Steady state
Velocity inlet	ABL (m/s) from [29]
Temperature inlet	40 °C
Relative humidity inlet	15 %
Pressure outlet	Atmospheric
Gravity	-9.81 m/s <sup>2</sup>
Walls	
Symmetry	Non-slip walls
Building (brick)	Density: 1000 kg/m <sup>3</sup> , C <sub>p</sub> : 1000 J/kgK, Thermal Conductivity: 0.15 W/mK
Ground (Ash solid)	Density: 1000 kg/m <sup>3</sup> , C <sub>p</sub> : 1000 J/kgK, Thermal Conductivity: 2 W/mK
	Spray settings [20,21]
Mass flow rate of water spray streams	3 L/min
Temperature of water spray streams	30 °C
Water flow velocity	15 m/s
Direction of water spray streams	Downward
	Droplet settings [20,21]
Number of droplet streams	300
Droplet diameter distribution model	Rosin-Rammler model
Number of diameters per droplet stream	20
Maximum diameter	518 μm
Minimum diameter	74 μm
Mean diameter	369 μm
Spread parameter	3.67

mm. Among these, the atrium model which featured a roof, was 52 mm high and had a roof slope angle of 22°. Four types of models were selected for CFD validation in this study: Model 1 was characterized by an open courtyard design, featuring a square plan configuration without a roof structure. Model 2 was designed as an atrium with a mono-pitch roof, devoid of any openings on the roof surface. Models 3 and 4 were both configured as mono-pitch roof atriums, featuring apertures on both windward and leeward sides of the roof, each with a window-to-wall ratio of 11.4 %. Given that this study focused on courtyard building, the courtyard model used in subsequent simulations was based on modifications of Model 1.

Through the comprehensive CFD modelling validation, accurate modelling and simulation assessments were conducted for all four models, including aspects such as the wind tunnel working section, geometry and dimensions of the models, window-to-wall ratio, and boundary conditions. Wind directions of 0° and 45° were applied to each model. Sharples and Bensalem applied an orifice plate to measure the rate of airflow through the model. The measurements involved recording the pressure drop across the orifice plate while simultaneously capturing dynamic pressure within the tunnel at the boundary layer height of 800 mm using a pitot-static tube. These dynamic pressure measurements facilitated the derivation of the reference wind speed at the top of the boundary layer, denoted as  $V_{800}$ , in their experiment measured at 25 m/s [29]. The standard orifice flow equation (Eq. (11)) was employed to estimate the flow rate  $Q$  through an opening of flow

area  $A$ .  $C_d$  is the discharge coefficient of the opening,  $\Delta p$  denotes the pressure difference across the opening, and  $\rho$  stands for air density. The air velocity at the orifice plate opening,  $V_0$  can be derived from Eq. (11) as  $Q/A$ . Given the known values of  $Q$  and  $A$ ,  $V_0$  can be determined accordingly [29]. Sharples and Bensalem also introduced a new dimensionless coefficient ( $CQ_t$ ) in their experiment, which was calculated as shown in Eq. (12):

$$Q = C_d A \left( \frac{2\Delta p}{\rho} \right)^{0.5} \quad (11b)$$

$$CQ_t = \frac{1}{N} \sum_{i=1}^N \frac{V_0}{V_{800}} \quad (12)$$

As shown in Fig. 6 and Table A1, it can be concluded that the experimental and numerical results are consistent, with similarities exceeding 80 %. Particularly at 0° wind direction, the numerical results for Models 1, 2, and 3 align well with the experimental results. The errors between the experiments for Models 1 and 2 and the CFD simulations are both less than 5 %, while the performance of Model 3 at 0° wind direction is particularly notable, the CFD accurately reflects the  $CQ_t$  in the wind tunnel experiment. However, the performance of Model 4, featuring a windward opening, at 0° wind direction is relatively moderate, with errors between the experiment and simulation reaching 18.54 %. Nonetheless, this error rate is still considered to be within an acceptable range.

Compared to the 0° wind direction, performance at 45° wind direction is slightly less accurate, with an average error of approximately 11.77 % among the four models; notably, the error of the open courtyard Model 1 is 11.18 %. From the validation results, it is evident that, at a 0° wind direction, the CFD simulation results are more accurate. However, it must be acknowledged that some degree of error is inevitable when CFD is used to predict wind tunnel experimental results. This is partly because CFD cannot fully replicate the exact boundary conditions set in the wind tunnel experiments, and there may also be errors inherent to experimental measurements themselves. Despite these discrepancies, a similarity exceeding 80 % is acceptable. Notably, the subsequent simulation models, which are based on modifications of Model 1 at a 0° wind direction, exhibit an error of only 2.33 %. These validation errors underscore effectiveness of CFD in accurately predicting wind tunnel experimental results, further emphasizing the reliability and accuracy of subsequent simulation studies.

### 3.2. Validation of the water sprayer model

The validation of the evaporative cooling sprayer, based on earlier works [19,21], sought to assess the cooling jet characteristics in CFD. This study conducted a comprehensive evaluation of the Lagrangian-Eulerian approach for evaporative cooling using a water spraying system equipped with a hollow cone nozzle. The validation was conducted in a computational domain measuring 0.585 m × 0.585 m × 1.9 m, with a scaled-down hollow cone nozzle of 4 mm diameter, as depicted in Fig. 7 (a), which illustrates the wind tunnel test setup [19]. The CFD validation encompassed boundary conditions, spray jet

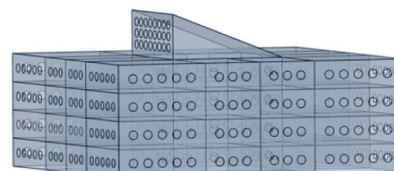
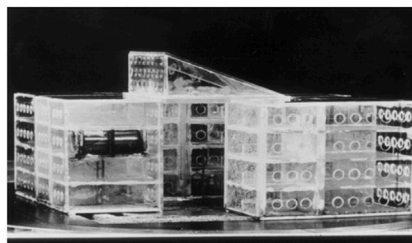


**Fig. 5.** Visual comparison between the wind tunnel experimental model (left) [29], and the geometry of the CFD model (right) utilized for validation.

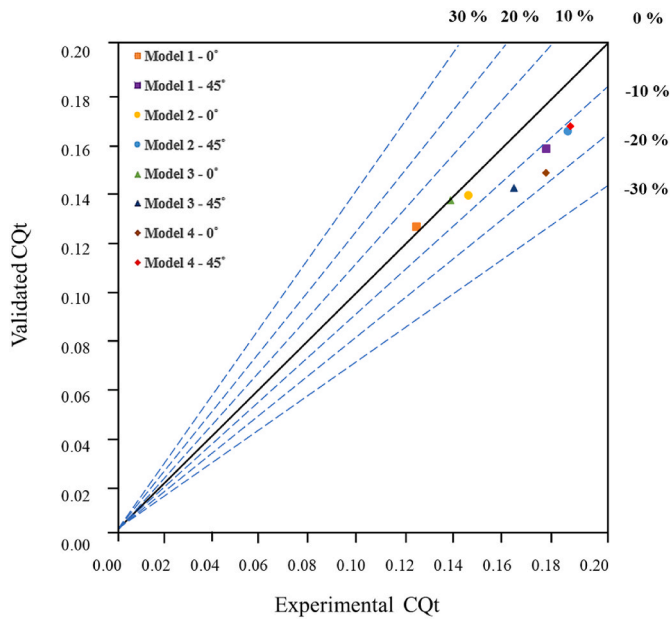


Fig. 6. Deviation analysis for wind tunnel experiments and numerical simulations in the courtyard and atriums.

properties, droplet characteristics, and solver settings in line with [21], Fig. 7 (b) and Fig. 7 (c) compare the current CFD results with previous data, with a focus on wind velocity and temperature along a central cross-section vertical line. In proximity to the nozzle at  $X = 0.1$  m, the validation exhibited high consistency in wind velocity and temperature with prior results. As the distance from the nozzle increased, wind velocity measurements were slightly higher, especially below the nozzle and near the fluid domain's upper boundary, while temperature readings were marginally lower than in previous studies. These trends were in complete agreement with past findings, with minor variations potentially attributed to differences in boundary condition settings and grid processing between the current and previous studies, affirming the high consistency between the two datasets.

### 3.3. Single-sided ventilated courtyard: wind and thermal performance with and without water sprayers

The airflow patterns around the single-sided ventilated courtyard building, as illustrated in Fig. 1(a) and Fig. A3, demonstrate the wind approaching from the inlet boundary on the left-hand side (the west side). A portion of the air ascends along the windward facade to the top of the building. The flow then splits, with some of the air entering the courtyard and some passing over, and then exiting to the pressure outlet on the right-hand side. A large recirculation region can be observed on the leeward side of the building. Within the single-sided ventilated courtyard, the behavior of the upper-level airflow can be described in terms of two primary directions. The predominant portion of the flow, known as the skimming flow, occurs at the windward edge and creates a negative pressure region above the courtyard with a magnitude of approximately  $-85$  Pa, preventing this airflow segment from penetrating the courtyard, as shown in Fig. A3 (a). This phenomenon is attributed to the interaction between the building's height and the wind pressure differential at the upper level. Consequently, this skimming flow does not return to the courtyard but instead continues along the roof's edge, contributing to the creation of negative pressure. The remaining airflow, affected by the courtyard's aspect ratio and the negative pressure induced by the skimming flow, is diverted downwards into the courtyard itself. This stream of air is guided along the courtyard's walls, leading to a complex pattern of circulation that includes upward motion and the formation of a vortex within the courtyard space. This vortex

plays a crucial role in enhancing ventilation effectiveness by drawing fresh outdoor air into the interior spaces, as indicated by the courtyard's internal pressure, which measures around  $-70$  Pa.

Fig. 8 (a) presents the average indoor wind velocity for 16 monitored rooms in the absence of water spraying devices. Notably, rooms on the west side exhibit the highest average wind velocity at  $0.231$  m/s. Specifically, the ground floor's RWG room experiences the highest wind velocity at  $0.329$  m/s. This is followed by rooms on the east side, which have an average velocity of  $0.179$  m/s as the incoming airflow encounters the opposite east side wall, leading to a change in the wind's direction due to the wall's resistance. This change generates a clockwise-rotating vortex within the center of the courtyard. As this vortex impacts the west side rooms, the resulting dynamic pressure difference due to the collision and redirection contributes to the entry of part of the airflow into the RWG room, thereby increasing its wind velocity. The vortex then ascends along the wall of the west side rooms and eventually exits over the top of the courtyard. Consequently, this vortex facilitates the entry of a portion of the wind into the rooms on both the east and west sides, enhancing the indoor wind velocity of these rooms.

However, the rooms on the south and north sides experience lower wind velocities, as exemplified by the RSG and RNG rooms, with velocities of only  $0.044$  m/s and  $0.041$  m/s, respectively. The observation is based on the fact that when the entering wind collides with the east side wall, it generates a vortex. The primary dynamic force of the airflow concentrates along the direction of the vortex's formation, i.e., the east-west direction. The motion of the vortex intensifies airflow along its axial direction, whereas in directions perpendicular to the vortex's axis (south-north direction), the airflow disperses, which reduces wind velocities. Furthermore, since the vortex predominantly moves in the east-west direction, the south and north side rooms, which do not directly face the main wind entrance, receive less dynamic airflow. Compared to the direct ventilative effect observed in the east and west side rooms, the south and north side rooms rely primarily on the secondary distribution of airflow for ventilation.

Within the courtyard building with water sprayers, variations in wind velocity across different orientations has been observed. As illustrated in Fig. 8 (b) rooms on the northern side demonstrate the highest average wind velocity, recorded at  $0.201$  m/s, with the third-floor RST room reaching a wind speed of  $0.419$  m/s. This indicates a significant influence of the water sprayers on the upper-level rooms facing north. Similarly, rooms on the southern side exhibit relatively high wind velocities, with an average speed of  $0.194$  m/s, while the third-floor RNT room achieves a wind speed of  $0.406$  m/s. In contrast, rooms on the western side present the lowest average wind velocity at a mere  $0.017$  m/s, and the ground-floor RWG room has the minimal recorded wind velocities of  $0.010$  m/s. The eastern side rooms have slightly higher wind velocities, averaging  $0.051$  m/s, with the third-floor RET room having a wind speed of  $0.042$  m/s.

A comparative analysis of wind speed contour maps for each room, as shown in Fig. 8 (a) and Fig. 8 (b), along with the wind speed comparison in Fig. 9 following the installation of water sprayers, reveals substantial changes in ventilation within the courtyard building. Out of the 16 monitored rooms, 8 exhibited increased wind speeds, all located on the southern and northern sides. The average wind speed in the northern rooms rose from  $0.043$  m/s without sprayers to  $0.201$  m/s with sprayers, with a surge on the third-floor RNT room from  $0.036$  m/s to  $0.406$  m/s. Conversely, 8 rooms, predominantly within the east and west-facing rooms, experienced a decrease in wind speed. The western rooms, particularly the ground-floor RWG room, witnessed a drastic drop from  $0.329$  m/s to  $0.010$  m/s. The average wind speed in these western rooms decreased by approximately  $0.214$  m/s, while the eastern rooms, less drastically affected, saw an average decrease of  $0.127$  m/s. Moreover, the second floor exhibited the most notable change in wind velocity after the water sprayer installation, with an increase of approximately  $0.094$  m/s.

A series of notable changes were observed in a detailed comparative



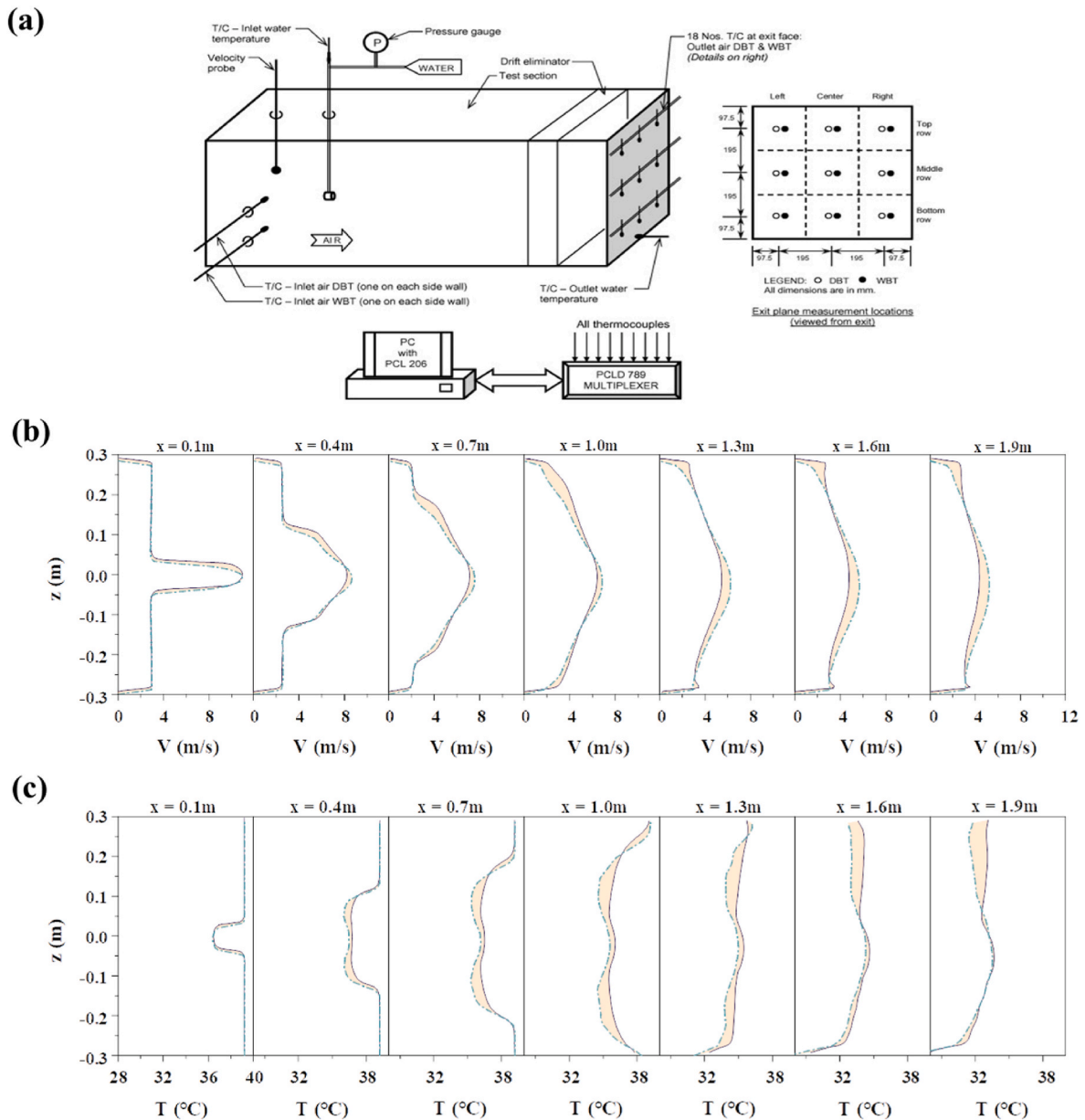


Fig. 7. (a) Wind tunnel test setup for the evaporative cooling water sprayer [19]. Comparative analysis of (b) air velocity and (c) temperature profile along a vertical centre plane lines between CFD results and experimental data from Ref. [21]. Representation key: dashed line for current validation results; solid black line for previous findings.

analysis of ventilation effects before and after water sprayer installation in courtyard building. Before the installation, rooms on the east and west sides, positioned along the primary movement path of the courtyard's vortex, exhibited higher average wind speeds compared to the north and south sides, which depend on secondary airflow distribution. However, post-installation, there was a marked increase with increased wind speeds on the north and south-facing rooms and a decrease in the east and west sides. Two key factors contributed to this change:

- (i) While the fundamental motion pattern of the courtyard's vortex remained unchanged, the introduction of water spraying devices and the resultant mist created obstructions and diversions in the main airflow pathways. For instance, the RWG room, initially characterized by the highest wind speed, underwent a substantial impact, likely due to the obstruction caused by the water sprayers. Consequently, the vortex within the courtyard, disrupted by the water sprayers, redirected a greater volume of

airflow towards the north and south sides, which increased wind speeds in these directions.

- (ii) The evaporative cooling effect induced by the water sprayers led to a reduction in air temperature and increase humidity, consequently, an increase in air density. This denser, cooler air tended to move downwards, altering the natural airflow patterns within the courtyard. This mechanism explains the observed increase in wind speeds in the north and south rooms during the operation of the water sprayers, as they likely directed airflow towards these areas. The introduction of cooler air through evaporative spraying created local pressure differentials within the courtyard, influencing the direction and speed of the airflow. In configurations without water sprayers, natural wind patterns might dominate, leading to higher airflow in the east and west rooms. In contrast, the water spraying configuration could generate new pressure gradients and redirect the airflow towards the north and south rooms.

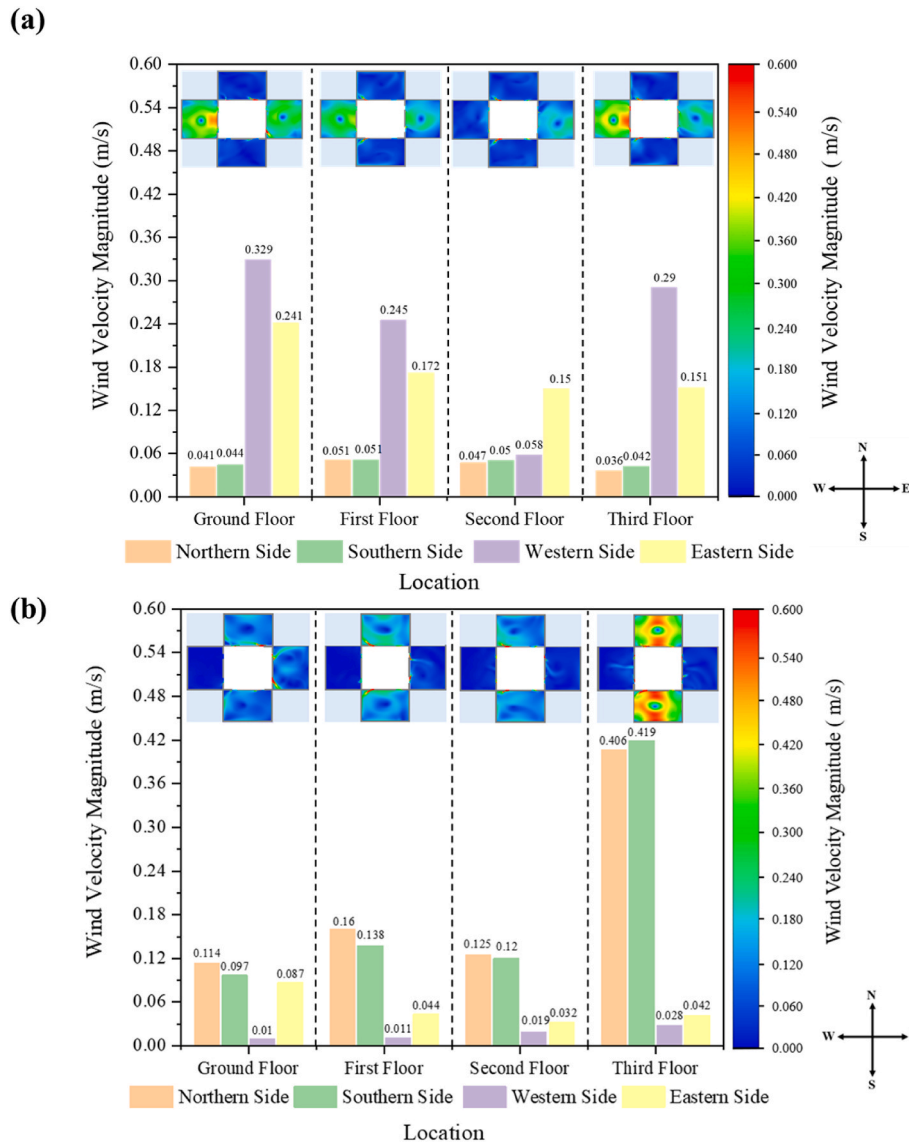


Fig. 8. Comparison of indoor wind velocity in the SSV courtyard (a) without and (b) with water sprayers, including cross-sectional velocity contours for each room.

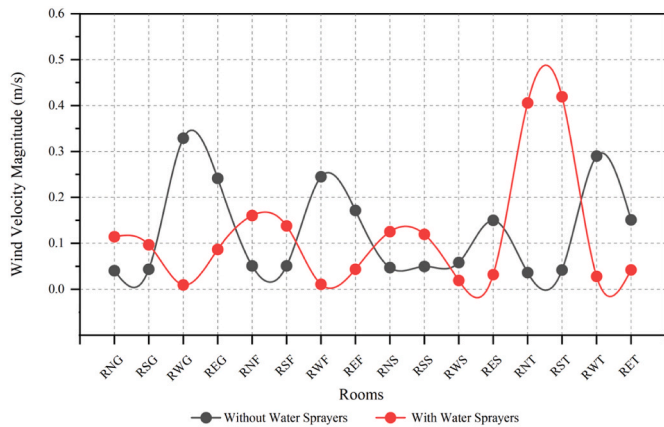
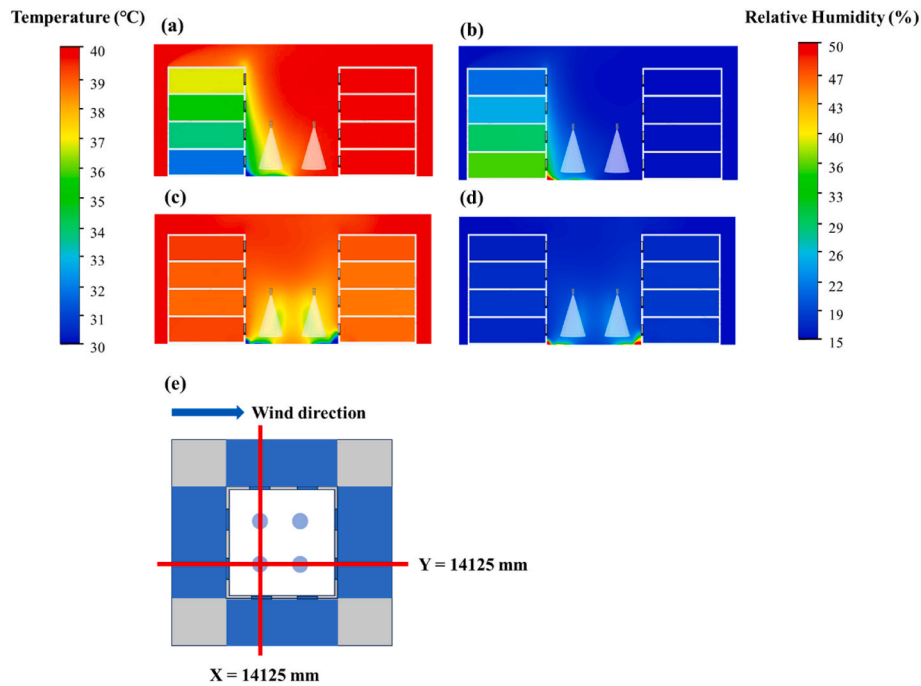


Fig. 9. Wind velocity comparison in each test room within the SSV courtyard with and without water sprayers.

To investigate the impact of water spraying on the indoor temperature and humidity of courtyard buildings, the inlet conditions were set to 40 °C and 15 % humidity without water spraying. The provided images

display the variations in temperature and humidity at different sections after the installation of water spraying devices. Fig. 10 (a) and Fig. 10 (b) show changes at the Y = 14125 mm cross-section, which corresponds to the west and east sides of the building, as well as the respective parts of the courtyard. Observations indicate a general decrease in temperatures in rooms on the west side, and this cooling effect gradually weakened with the increase in floor height. Notably, a concentration of cold air was observed outside the RWG room. However, temperature changes in rooms on the east side were minimal. The trend in humidity changes was similar to that of temperature, with the highest humidity observed in the RWG room. Furthermore, humidity in the rooms on the west side decreased with increasing height. Fig. 10 (c) and Fig. 10 (d) present the temperature and humidity changes at the X = 14125 mm section, which corresponds to the rooms on the north and south sides. Analysis of the figures reveals insignificant changes in indoor temperature and humidity in the north and south rooms, indicating limited cooling and humidifying effects of the water spraying devices in these directions. It is also noticeable that the main areas of temperature decrease, and humidity increase are concentrated around the water spraying devices and have not significantly propagated into the indoor areas, which implies that the influence of the water spraying devices is primarily confined to their immediate vicinity, with limited regulation exerted on the wider



**Fig. 10.** Temperature and relative humidity contours at two cross-sections within the SSV courtyard with water sprayers. (a) Temperature at cross-section Y = 14125 mm and (b) Relative humidity at cross-section Y = 14125 mm. (c) Temperature at cross-section X = 14125 mm and (d) relative humidity at cross-section X = 14125 mm. (e) Location of the cross-sections.

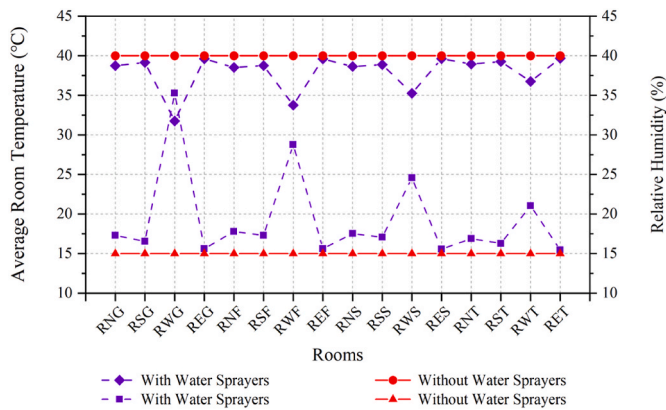


**Fig. 11.** Comparative graph of indoor temperature (Red) and relative humidity (Purple) levels in each room within the SSV courtyard, with and without water sprayers. (For interpretation of the references to colour in this figure legend, the reader is referred to the Web version of this article.)

indoor environment of the courtyard building.

Fig. 11 reveals the variations in temperature and humidity across different rooms before and after the installation of water spraying devices, indicating a correlation between indoor temperature and humidity. The data suggests that a decrease in temperature is often accompanied by an increase in humidity, with minor temperature changes corresponding to smaller shifts in humidity. Rooms on the west side, which experienced the most significant cooling, exhibited a substantial increase in humidity. The average temperature drops from 40 °C to 34.38 °C was accompanied by a rise in humidity to 27.42 %. Specifically, the ground-floor RWG room saw a temperature drop of 8.25 °C and a humidity increase of 20.27 %. In contrast, the east side, particularly the RET room, displayed a marginal temperature decrease of 0.32 °C, indicating a relatively weaker cooling and humidifying effect.

Combined with the temperature and humidity contour maps in Fig. 10, it is observable that the cooling and humidifying effects are not pronounced in the rooms on the east, south, and north sides. Moreover, the height of the floors also influenced the effectiveness of the water spraying devices.

An examination of the cooling and humidifying effects revealed a significant increase in temperature and humidity around the devices, consistent with the physical principles of evaporative cooling. As water evaporation requires heat absorption, the surrounding air temperature decreases, and the addition of water vapor also raises relative humidity. When the airflow enters the courtyard and comes into contact with the water-spraying devices, the warm air passing through the mist undergoes a cooling effect, albeit with a reduction in flow velocity. The main airflow in the courtyard follows a vortex structure. When the vortex-driven airflow directly hits the eastern rooms without any contact with the water sprayers, the cooling and humidifying effect in these rooms is weaker. Additionally, as the vortex-direction airflow strikes the eastern wall, it partially redistributes towards the south and north sides. However, due to the obstruction caused by the water sprayers, most of the airflow bypasses and enters the south and north rooms. This diversion results in an increase in wind speed without a significant reduction in temperature. In rooms with higher wind speeds, the cooler and more humid air may dissipate quickly, reducing the overall effects of cooling and humidification. Conversely, rooms on the west side, positioned in the main wind direction of the vortex core and directly exposed to the airflow from the water sprayers, experience the most notable cooling effect, particularly the RWG room, where a significant influx of cooled airflow achieves a temperature reduction of up to 8.25 °C. The lower wind speed inside the RWG room allows the cold air to linger for a longer period, which enhances the cooling effect. As the vortex ascends and departs the courtyard near the west side rooms, the cooling and humidifying effects gradually diminish with the increase in floor height, likely due to the tendency of cold air to sink and warm air to rise, leading to a relative weakening of the cooling effect in the upper rooms.

3.4. Cross-ventilated courtyard: wind and thermal performance with and without water sprayers

Compared to single-sided ventilation, the cross ventilation in the courtyard building presents significantly different airflow characteristics. The pattern of ventilation in courtyard buildings is shown in Fig. 1 (b). The wind approaches from the inlet boundary on the left-hand side, initially impacting the western windward side, which results in substantial airflow into the rooms facing west. Subsequently, some of this airflow moves directly into the center of the courtyard. Above the courtyard, the airflow diverges into two principal directions, a phenomenon referred to as skimming flow. This flow, characterized by its passage along the building's upper edges, establishes a distinct aerodynamic behaviour. The negative pressure above the courtyard is somewhat lower, measuring around -75 Pa, with the internal courtyard pressure being approximately -55 Pa, as illustrated in Fig. A3(b). One air stream initiates a downward motion, creating a vortex that extends deep into the courtyard—this is indicative of the skimming flow's influence as it redirects air vertically. Concurrently, another portion of the airflow, adhering to the path of the skimming flow, crosses the courtyard's centre and veers towards the eastern side. This action precipitates a considerable vortex formation on the leeward side of the building, a direct result

of the skimming flow as it moves across the building's surface. The ensuing vortex creates a unique circulation pattern, where a segment of the air bypasses the eastern structure, infiltrates the indoor spaces, and subsequently re-enters the courtyard. This interaction between the skimming flow and the courtyard's architectural features significantly enhances the complex internal airflow dynamics. Meanwhile, the courtyard building acts as a wind boundary, guiding part of the airflow along the north and south sides, with only a small amount entering the rooms on the north and south. In such a ventilation configuration, the airflow from inside to the courtyard is no longer the main channel for indoor air intake compared to the vortex within the courtyard.

Fig. 12 (a) displays the velocity magnitude and contour diagram of the indoor wind speed in various floors in the CV courtyard without water sprayers. The highest wind speeds are concentrated in the rooms on the west side, with an average wind speed of 1.236 m/s. Particularly, the RWT room on the third floor exhibits the highest wind speed of up to 1.283 m/s. The rooms on the east side, positioned on the leeward side, have an average wind speed of about 0.665 m/s, approximately half that of the west side. The average wind speeds of the rooms on the north and south sides are quite similar, both around 0.4 m/s. Upon the operation of the water sprayers, as shown in Fig. 12 (b), there is no significant change in the overall trend of wind speed distribution. The average wind speed

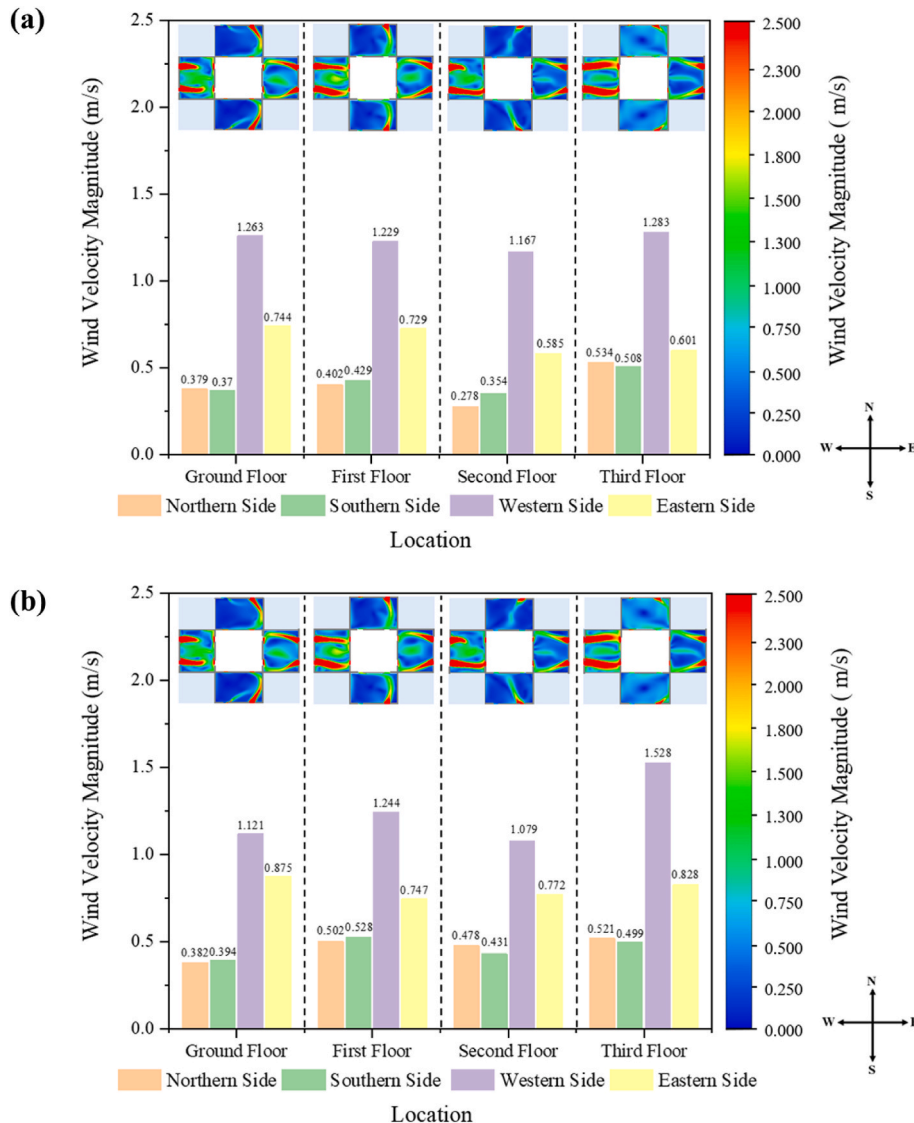


Fig. 12. Comparison of indoor wind velocity in the CV courtyard (a) without and with (b) water sprayers, including cross-sectional velocity contours for each room.

in the rooms on the west side remains the highest at 1.243 m/s, followed by the four rooms on the east side with an average wind speed of about 0.806 m/s. The comparison of indoor wind speeds before and after the introduction of water sprayers clearly shows that under cross flow ventilation, the impact of water sprayers in the courtyard on the indoor wind environment is negligible. This phenomenon indicates that under this ventilation mode, the main source of indoor airflow comes from the wind from outside the courtyard.

After the installation of water spraying devices in the courtyard building with cross ventilation design, data showed no changes in indoor temperature and humidity. The initial indoor conditions were set at 40 °C, with a relative humidity of 15 %. This phenomenon revealed that under such ventilation strategy, indoor air is primarily drawn from the outside of the courtyard and then flows through the indoor space before its recirculated back to the courtyard, see Fig. 1 (b). Consequently, the water spraying devices in the courtyard have a limited role in the heat exchange process as they fail to effectively cool and humidify the hot air. It can be inferred that in courtyard buildings with a cross flow ventilation mode, the installation of water spraying devices contributes minimally to improving the indoor thermal and humidity environment (as shown in Fig. 13 and Table 3).

#### 4. Discussion and limitations

##### 4.1. Water flow rate

To investigate the impact of varying evaporative cooling system water flow rates on the indoor thermal control in the single-sided ventilated courtyard building, this study systematically analyzed 13 different flow rates ranging from 0.5 l/min to 12 l/min. Maintaining constant water temperature and velocity, the study focused on single-sided ventilated courtyards, which demonstrated a more significant cooling effect compared to courtyards with cross flow ventilation. There is a clear trend shown in Fig. 14 (a), as the water flow rate increases, the distribution of average temperatures within buildings surrounding the courtyard gradually expands. This finding indicates that increasing the water flow rate has a significant cooling effect on certain rooms, while for others, this cooling effect is less pronounced. In other words, increasing the water flow rate can effectively improve the temperature conditions in certain spaces, but the effect is not uniform, reflecting the differences in how various rooms respond to cooling measures. The results presented in Fig. A4 shows the effectiveness of water sprayers in the reducing the room air temperature. Notably, the cooling effect progressively intensifies as the water flow rate increases.

Detailed observation of temperature reductions across different rooms revealed the most significant change in the RWG room on the

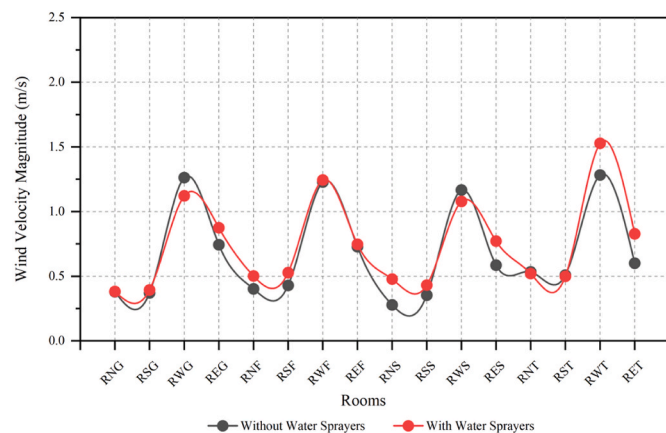


Fig. 13. Wind velocity comparison in each test room within the CV courtyard with and without water sprayers.

Table 3

Average indoor temperature and relative humidity of the CV courtyard with water sprayers.

Rooms	Temperature (°C)	RH (%)
	With water sprayers	With water sprayers
RNG	40.00	15.00
RSG	40.00	15.00
RWG	40.00	15.01
REG	39.99	15.03
RNF	40.00	15.00
RSF	40.00	15.00
RWF	40.00	15.00
REF	39.99	15.03
RNS	40.00	15.00
RSS	40.00	15.00
RWS	40.00	15.01
RES	39.99	15.03
RNT	40.00	15.00
RST	40.00	15.00
RWT	40.00	15.01
RET	39.99	15.03

ground floor, where the temperature dropped by 2.70 °C at a flow rate of 0.5 l/min and 13.93 °C at 12 l/min. This finding highlights the enhanced cooling capacity of water sprayers with increasing flow rates, particularly in the RWG room. Overall, the west-facing rooms experienced the most notable cooling effects, while the east-facing rooms exhibited minimal change even with increased flow rates. Additionally, the cooling effects in the north and south-facing rooms varied with the flow rates. For instance, in the RNG room, the temperature decrease ranged from 1.26 °C to 3.39 °C when the flow rate increased from 3 l/min to 4 l/min. A further increase from 5 l/min to 6 l/min raised the cooling effect from 3.08 °C to 8.53 °C, suggesting that higher water flow rates might alter the wind field within the courtyard, benefiting both the west and north-facing rooms simultaneously.

However, irrespective of water flow rate changes, east-facing rooms showed no cooling, indicating that the indoor airflow in single-sided ventilated courtyard buildings is mainly influenced by large courtyard vortices. The diminishing cooling effect with increased floor height also corresponds to the physical property of cold air being denser and accumulating at lower levels. As displayed in Fig. 14 (b), the average temperature across all rooms shows a trend of gradual decrease with increasing water flow rates, this trend stabilizes beyond the flow rates of 10 l/min, 11 l/min, and 12 l/min. This stabilization of temperature reduction corresponds to the physical limit of evaporative cooling efficiency. Beyond a certain water flow rate, the air reaches a moisture content at which it cannot effectively absorb more water vapor, leading to a state of saturation. Thus, while increasing the flow rate initially improves cooling due to enhanced evaporation, the effect becomes less pronounced as the air's capacity for vapor absorption nears its limit.

##### 4.2. Limitations

In this study, we conducted a comprehensive analysis of the impact of water sprayers in courtyard buildings under different ventilation strategies using CFD simulations. Despite the key findings obtained, it is crucial to acknowledge the limitations of the research process. The operation and positioning of water sprayers in this study may not accurately represent the diverse configurations found in real-world settings. The simulations, with their constant water temperature and water flow rate, may fall short of modelling the dynamic conditions that influence the performance of sprayers. Additionally, the ventilation strategies explored here may not encompass the range of approaches applied in actual environments. The occurrence of errors between wind tunnel experiments and CFD simulations is inevitable, primarily attributed to the complex nature of the model and external factors. Moreover, our study exclusively utilizes simplified wind tunnel models for CFD simulations, which may overlook critical complex factors present in real-

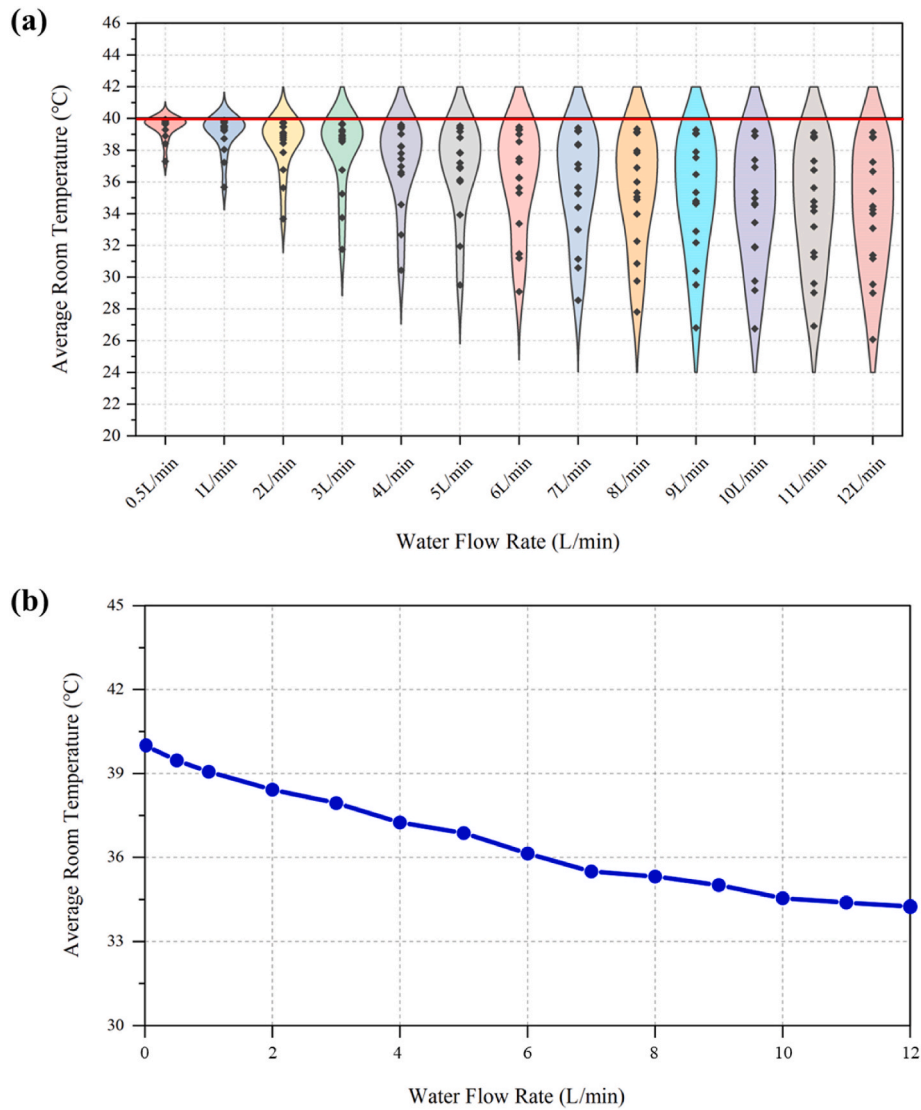


**Fig. 14.** Comparison of indoor average temperature changes for varying water flow rates in the SSV courtyard: (a) variations of indoor temperature across the rooms, the red line represents the outdoor temperature and (b) overall average room temperature. (For interpretation of the references to colour in this figure legend, the reader is referred to the Web version of this article.)

world environments.

### 5. Conclusion and future works

This study investigates the impact of evaporative cooling from water sprayers in courtyard buildings under different ventilation strategies on the indoor thermal environment and microclimate. Although the influence of passive techniques on courtyards has been widely studied, their specific impact on the indoor thermal environment of courtyard buildings remains relatively unexplored, which constitutes the innovative focus of this study. With CFD analysis and validation through wind tunnel experiment, the study focused on courtyard buildings with two different ventilation strategies, each featuring uniformly distributed water sprayers.

In courtyard buildings with single-side ventilation, the introduction of water sprayers induced significant changes in the indoor wind environment, primarily due to the obstruction of incoming wind by sprayers and alterations in air movement direction caused by changes in temperature and humidity. The most significant cooling effect of up to 8.25 °C and a humidity increase of 20.27 % were observed in the ground-floor rooms on the west side. On average, the temperature in the

16 test rooms decreased by 2.06 °C, and the relative humidity increased by 4.29 %. The cooling effect was predominantly observed in the west-facing rooms and gradually diminished with rising floor levels. In contrast, in courtyard buildings with cross-ventilation, the impact of water sprayers on the indoor thermal environment was relatively modest, with minimal changes in the indoor wind environment and cooling-humidifying effects.

This study analyzed the impact of different water flow rates, ranging from 0.5 l/min to 12 l/min, on indoor thermal control in a single-sided ventilated courtyard building. A notable temperature reduction in certain rooms was observed when the water flow rate increased from 5 l/min to 6 l/min. However, further increases in water flow rate led to a saturation of the indoor cooling effect. Overall, the study emphasizes the potential of evaporative cooling strategies in improving thermal conditions in courtyard buildings, especially in hot and dry climates, while also underscoring the need for tailored solutions based on specific building features and environmental conditions. This study lays a solid foundation for further research under varying ventilation strategies and water flow rates.

Future works, based on the identified limitations in the current study, will expand and adjust our existing model, which involves

adjustments to the position, height, and water temperature of the water sprayers to investigate deeper into their impact on the indoor thermal environment of the courtyard buildings. Additionally, our previous research revealed that evaporative cooling techniques in single-sided ventilated courtyard buildings significantly affect only specific areas. Conversely, in cross-ventilated courtyard buildings, they did not improve the indoor thermal and humidity environment across all rooms. Future studies aim to extend these cooling and humidifying effects to a broader range of rooms. For instance, we could adopt a similar approach to that referenced in ref. [38], which employed evaporative cooling strategies directly at the inlet of the building. This could potentially remedy the limitations observed in cross flow ventilation configurations, where indoor air is predominantly drawn from outside the building.

Another critical aspect of future research will entail transitioning from wind tunnel-based courtyard models to simulations based on real-life courtyard buildings. This will involve integrating actual weather data into the simulations, thereby enhancing realism and applicability. By simulating scenarios based on real-world conditions, we can better capture the complexities of air-thermal interactions within courtyard environments, thus increasing the accuracy and relevance of our findings.

Finally, in this study, the RANS turbulence model (specifically the k-epsilon Realizable model) was primarily selected for its adequacy in meeting basic requirements for validating courtyard and water spray simulations, coupled with its cost-effectiveness in computational resources. However, future research will undertake a comparative analysis of the accuracy of transient large eddy simulation (LES) models to determine if they offer a more precise understanding of the microclimatic conditions within courtyard environments. This comparison is anticipated to provide valuable insights into the selection of appropriate simulation models for different research objectives.

Nomenclature

Abbreviation	
UHI	Urban Heat Island
CFD	Computational Fluid Dynamics
CV	Cross Ventilated
SSV	Single-Sided Ventilated
DPM	Discrete Phase Model
ABL	Atmospheric Boundary Layer
RH	Relative Humidity
RNG	Room - Northern - Ground Floor
RSG	Room - Southern - Ground Floor
RWG	Room - Western - Ground Floor
REG	Room - Eastern - Ground Floor
RNF	Room - Northern - First Floor
RSF	Room - Southern - First Floor
RWF	Room - Western - First Floor
REF	Room - Eastern - First Floor
RNS	Room - Northern - Second Floor
RSS	Room - Southern - Second Floor
RWS	Room - Western - Second Floor
RES	Room - Eastern - Second Floor
RNT	Room - Northern - Third Floor
RST	Room - Southern - Third Floor
RWT	Room - Western - Third Floor
RET	Room - Eastern - Third Floor
RANS	Reynolds-Averaged Navier-Stokes
LES	Large Eddy Simulation
Symbols	
$\rho$	Density (kg/m <sup>3</sup> )
$t$	Time
$u$	Velocity (m/s)
$p$	Pressure (Pa)
$g$	Gravitational acceleration (m/s <sup>2</sup> )
$\tau$	Stress tensor (Pa)
$E$	Energy (J)

(continued on next column)

(continued)

$\kappa$	Thermal conductivity (W/m-K)
$k$	Turbulent kinetic energy (m <sup>2</sup> /s <sup>2</sup> )
$\epsilon$	Dissipation rate (m <sup>3</sup> /s <sup>3</sup> )
$\mu$	Molecular viscosity (Pa·s)
$\sigma$	Prandtl numbers
$S$	User-defined source terms (kg/m <sup>3</sup> ·s, J, m <sup>2</sup> /s <sup>2</sup> , m <sup>3</sup> /s <sup>3</sup> )
$Y$	Mass fraction
$J$	Diffusion flux (mol/m <sup>2</sup> ·s)
$R$	Rate of reaction (mol/L·s)
$F$	External body force (N)
$N$	Mass transfer rate (kg/s)
$A$	Area (m <sup>2</sup> )
$C$	Concentration (mol/m <sup>3</sup> )
$Sh$	Sherwood number
$d$	Diameter (m)
$Re$	Reynolds number
$S_c$	Schmidt number
$L$	L Length (m)
$W$	Width (m)
$H$	Height (m)
$Z$	Height at Z (m)
$\alpha$	Power law exponent
$C_p$	Specific heat (J/kg·K)
$CQ_t$	User-defined dimensionless velocity coefficient
Subscript	
eff	Effective
$h$	Heat
$k$	Turbulence kinetic energy
$\epsilon$	Dissipation rate
$i$	Species
$d$	Droplet
$m$	Mass
$\infty$	Free stream
ref	Reference
$o$	Opening

Disclosure statement

No potential conflict of interest is reported by the authors.

CRedit authorship contribution statement

**Hao Sun:** Writing – original draft, Visualization, Validation, Software, Methodology, Investigation, Formal analysis, Data curation, Writing – review & editing. **Hua Zhong:** Writing – review & editing, Validation, Formal analysis. **Abdullah Dik:** Methodology, Investigation, Conceptualization, Formal analysis, Visualization, Writing – original draft, Validation, Writing – review & editing. **Kemin Ding:** Validation, Formal analysis, Methodology. **Carlos Jimenez-Bescos:** Supervision. **John Kaiser Calautit:** Writing – review & editing, Validation, Supervision, Project administration, Methodology, Investigation, Formal analysis, Conceptualization.

Declaration of competing interest

The authors declare that they have no known competing financial interests or personal relationships that could have appeared to influence the work reported in this paper.

Data availability

Data will be made available on request.

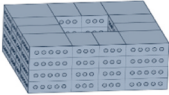
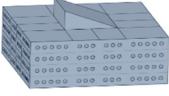
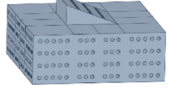
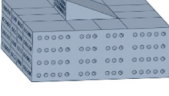
Acknowledgement

The authors would like to thank the support of the Department of Architecture and Built Environment of the University of Nottingham for providing the facility for carrying out the modelling and simulations.

Appendix

Table A.1

Velocity coefficient  $C_{Q_t}$  validation results for the courtyard and atriums numerical simulation.

Model	Models	Wind direction (°)	Experimental $C_{Q_t}$ [29]	Current $C_{Q_t}$	Error (%)
Model 1		0	0.126	0.129	2.33
		45	0.179	0.161	11.18
Model 2		0	0.147	0.142	3.52
		45	0.188	0.168	11.90
Model 3		0	0.140	0.140	0
		45	0.166	0.145	14.48
Model 4		0	0.179	0.151	18.54
		45	0.189	0.171	9.52

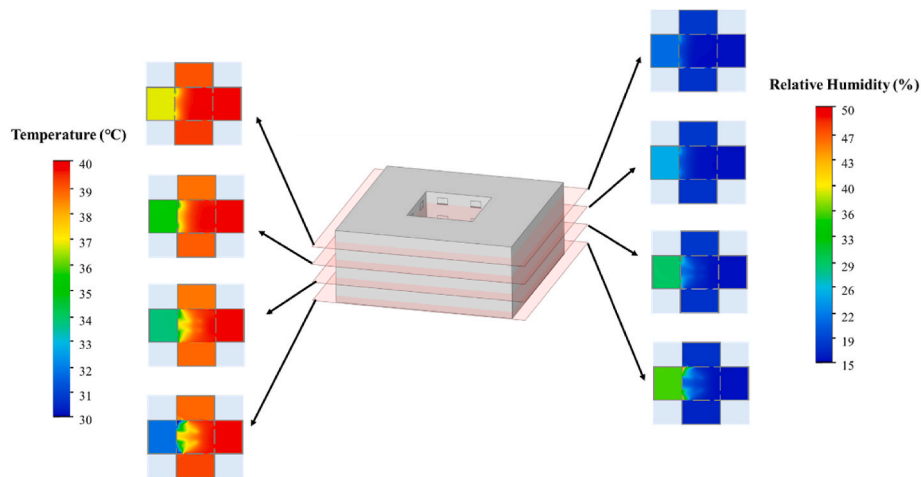


Fig. A.1. Temperature and relative humidity contours for each floor in the SSV courtyard with water sprayers (sectioned at the window openings).

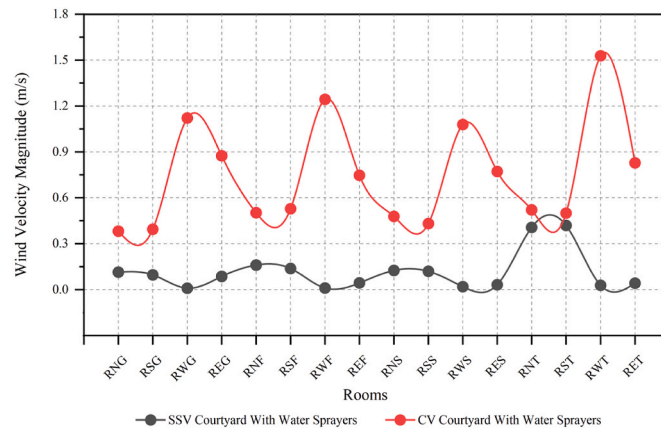


Fig. A.2. Wind velocity comparison in each test room for the SSV and CV courtyards with water sprayers.



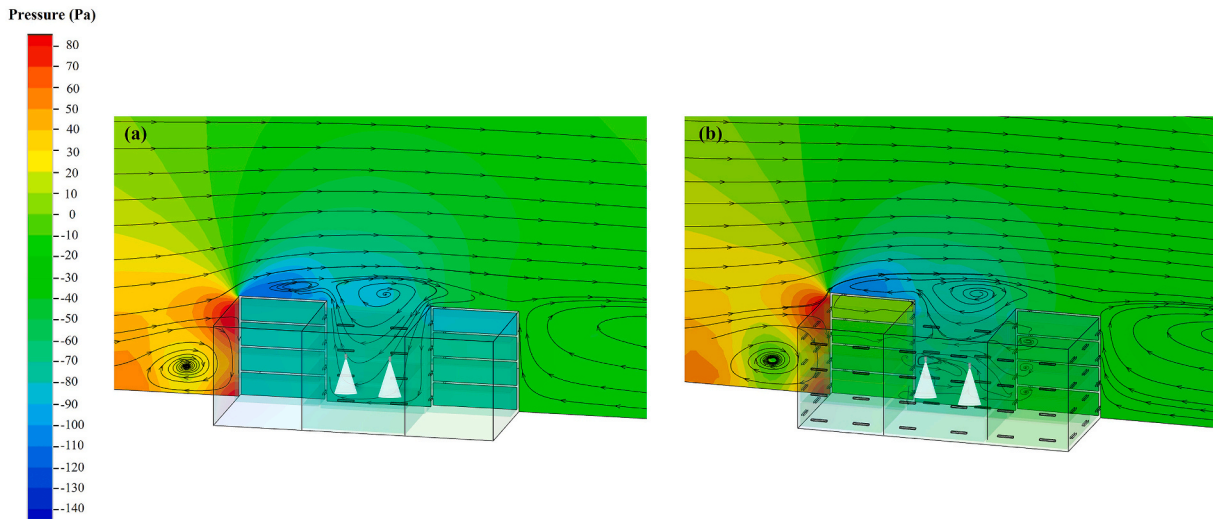


Fig. A.3. Comparative visualization of courtyard ventilation strategies at Y = 14125 mm section: (a) SSV courtyard with water sprayers, (b) CV courtyard with water sprayers.

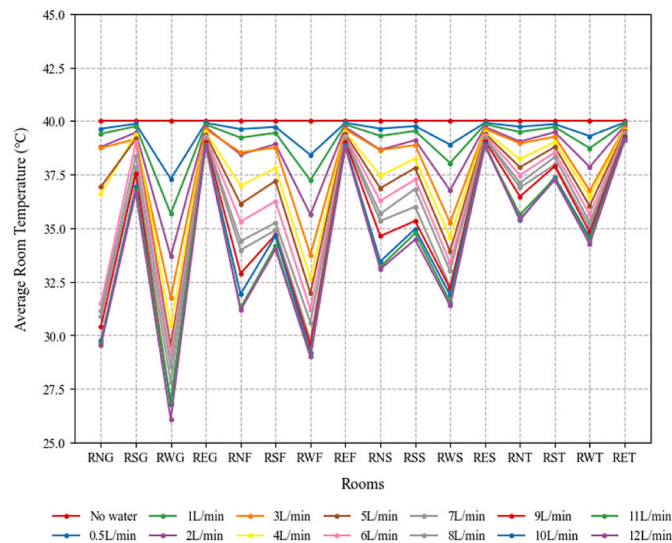


Fig. A.4. Comparison of indoor average temperature changes for varying water flow rates in the SSV courtyard.

References

- [1] Y.H. Yau, S. Hasbi, A review of climate change impacts on commercial buildings and their technical services in the tropics, *Renew. Sustain. Energy Rev.* 18 (2013) 430–441, <https://doi.org/10.1016/j.rser.2012.10.035>.
- [2] M. Hamdy, S. Carlucci, P.-J. Hoes, J.L.M. Hensen, The impact of climate change on the overheating risk in dwellings—a Dutch case study, *Build. Environ.* 122 (2017) 307–323, <https://doi.org/10.1016/j.buildenv.2017.06.031>.
- [3] Z. Yilmaz, Evaluation of energy efficient design strategies for different climatic zones: comparison of thermal performance of buildings in temperate-humid and hot-dry climate, *Energy Build.* 39 (2007) 306–316, <https://doi.org/10.1016/j.enbuild.2006.08.004>.
- [4] H. Sun, J.K. Calautit, C. Jimenez-Bescos, Examining the regulating impact of thermal mass on overheating, and the role of night ventilation, within different climates and future scenarios across China, *Clean. Eng. Tech.* 9 (2022) 100534, <https://doi.org/10.1016/j.clet.2022.100534>.
- [5] E. Diz-Mellado, Á. Ruiz-Pardo, C. Rivera-Gómez, F.J. Sanchez De La Flor, C. Galán-Marín, Unravelling the impact of courtyard geometry on cooling energy consumption in buildings, *Build. Environ.* 237 (2023) 110349, <https://doi.org/10.1016/j.buildenv.2023.110349>.
- [6] X. Cao, X. Dai, J. Liu, Building energy-consumption status worldwide and the state-of-the-art technologies for zero-energy buildings during the past decade, *Energy Build.* 128 (2016) 198–213, <https://doi.org/10.1016/j.enbuild.2016.06.089>.
- [7] M. Isaac, D.P. van Vuuren, Modeling global residential sector energy demand for heating and air conditioning in the context of climate change, *Energy Pol.* 37 (2009) 507–521, <https://doi.org/10.1016/j.enpol.2008.09.051>.
- [8] S. Moghimi, F. Azizpour, S. Mat, C.H. Lim, E. Salleh, K. Sopian, Building energy index and end-use energy analysis in large-scale hospitals—case study in Malaysia, *Energy Efficiency* 7 (2014) 243–256, <https://doi.org/10.1007/s12053-013-9221-y>.
- [9] H. Sun, C. Jimenez-Bescos, M. Mohammadi, F. Zhong, J.K. Calautit, Numerical investigation of the influence of vegetation on the aero-thermal performance of buildings with courtyards in hot climates, *Energies* 14 (2021) 5388, <https://doi.org/10.3390/en14175388>.
- [10] I. Rajapaksha, H. Nagai, M. Okumiya, A ventilated courtyard as a passive cooling strategy in the warm humid tropics, *Renew. Energy* 28 (2003) 1755–1778, [https://doi.org/10.1016/S0960-1481\(03\)00012-0](https://doi.org/10.1016/S0960-1481(03)00012-0).
- [11] N. Al-Masri, B. Abu-Hijleh, Courtyard housing in midrise buildings: an environmental assessment in hot-arid climate, *Renew. Sustain. Energy Rev.* 16 (2012) 1892–1898, <https://doi.org/10.1016/j.rser.2012.01.008>.
- [12] Z. Zamani, S. Heidari, P. Hanachi, Reviewing the thermal and microclimatic function of courtyards, *Renew. Sustain. Energy Rev.* 93 (2018) 580–595, <https://doi.org/10.1016/j.rser.2018.05.055>.
- [13] J.M. Rojas, C. Galán-Marín, E.D. Fernández-Nieto, Parametric study of thermodynamics in the mediterranean courtyard as a tool for the design of eco-efficient buildings, *Energies* 5 (2012) 2381–2403, <https://doi.org/10.3390/en5072381>.

- [14] R. Ernest, B. Ford, The role of multiple-courtyards in the promotion of convective cooling, *Architect. Sci. Rev.* 55 (2012) 241–249, <https://doi.org/10.1080/00038628.2012.723400>.
- [15] F. Soflaei, M. Shokouhian, S.M. Mofidi Shemirani, Investigation of Iranian traditional courtyard as passive cooling strategy (a field study on BS climate), *Int. J. Sustain. Built Environ.* 5 (2016) 99–113, <https://doi.org/10.1016/j.ijsbe.2015.12.001>.
- [16] Y.-B. Cai, Z.-J. Wu, Y.-H. Chen, L. Wu, W.-B. Pan, Investigate the difference of cooling effect between water bodies and green spaces: the study of fuzhou, China, *Water* 14 (2022) 1471, <https://doi.org/10.3390/w14091471>.
- [17] M.A.M.J. Noordin, N.C.M. Nasir, R.M. Nasir, D. Mustapa, New added values to the existing Chinese heritage shop-houses' courtyards towards occupant environment wellness: a case study at Kota Bharu, Kelantan, Malaysia, *IOP Conf. Ser. Earth Environ. Sci.* 738 (2021) 012055, <https://doi.org/10.1088/1755-1315/738/1/012055>.
- [18] S. Sahebzadeh, Z. Dalvand, M. Sadeghfar, A. Heidari, Vernacular architecture of Iran's hot regions; elements and strategies for a comfortable living environment, *SASBE* 9 (2018) 573–593, <https://doi.org/10.1108/SASBE-11-2017-0065>.
- [19] R. Sureshkumar, S.R. Kale, P.L. Dhar, Heat and mass transfer processes between a water spray and ambient air – I. Experimental data, *Appl. Therm. Eng.* 28 (2008) 349–360, <https://doi.org/10.1016/j.applthermaleng.2007.09.010>.
- [20] H. Montazeri, Y. Toparlar, B. Blocken, J.L.M. Hensen, Simulating the cooling effects of water spray systems in urban landscapes: a computational fluid dynamics study in Rotterdam, The Netherlands, *Landsc. Urban Plann.* 159 (2017) 85–100, <https://doi.org/10.1016/j.landurbplan.2016.10.001>.
- [21] H. Montazeri, B. Blocken, J.L.M. Hensen, Evaporative cooling by water spray systems: CFD simulation, experimental validation and sensitivity analysis, *Build. Environ.* 83 (2015) 129–141, <https://doi.org/10.1016/j.buildenv.2014.03.022>.
- [22] H. Montazeri, B. Blocken, J.L.M. Hensen, CFD analysis of the impact of physical parameters on evaporative cooling by a mist spray system, *Appl. Therm. Eng.* 75 (2015) 608–622, <https://doi.org/10.1016/j.applthermaleng.2014.09.078>.
- [23] F. Zhong, H.N. Chaudhry, J.K. Calautit, Effect of roof cooling and air curtain gates on thermal and wind conditions in stadiums for hot climates, *Energies* 14 (2021) 3941, <https://doi.org/10.3390/en14133941>.
- [24] M. Ghoulem, K. El Moueddeb, E. Nehdi, F. Zhong, J. Calautit, Analysis of passive draught evaporative cooling windcatcher for greenhouses in hot climatic conditions: parametric study and impact of neighbouring structures, *Biosyst. Eng.* 197 (2020) 105–121, <https://doi.org/10.1016/j.biosystemseng.2020.06.016>.
- [25] T. Ahmed, P. Kumar, L. Mottet, Natural ventilation in warm climates: the challenges of thermal comfort, heatwave resilience and indoor air quality, *Renew. Sustain. Energy Rev.* 138 (2021) 110669, <https://doi.org/10.1016/j.rser.2020.110669>.
- [26] H.-Y. Zhong, Y. Sun, J. Shang, F.-P. Qian, F.-Y. Zhao, H. Kikumoto, C. Jimenez-Bescos, X. Liu, Single-sided natural ventilation in buildings: a critical literature review, *Build. Environ.* 212 (2022) 108797, <https://doi.org/10.1016/j.buildenv.2022.108797>.
- [27] T.-H. Shih, W.W. Liou, A. Shabbir, Z. Yang, J. Zhu, A new k-ε eddy viscosity model for high Reynolds number turbulent flows, *Comput. Fluid* 24 (1995) 227–238, [https://doi.org/10.1016/0045-7930\(94\)00032-T](https://doi.org/10.1016/0045-7930(94)00032-T).
- [28] Ansys Fluent Theory Guide 2021R2, Ansys Inc., 2021. <https://www.ansys.com/>.
- [29] S. Sharples, R. Bensalem, Airflow in courtyard and atrium buildings in the urban environment: a wind tunnel study, *Sol. Energy* 70 (2001) 237–244, [https://doi.org/10.1016/S0038-092X\(00\)00092-X](https://doi.org/10.1016/S0038-092X(00)00092-X).
- [30] J. Franke, A. Hellsten, K. Schlünzen, B. Carissimo, *Model Evaluation Guidance and Protocol Document: COST Action 732 Quality Assurance and Improvement of Microscale Meteorological Models*, Univ. of Hamburg, Meteorological Inst, Hamburg, 2007.
- [31] Y. Tominaga, A. Mochida, R. Yoshie, H. Kataoka, T. Nozu, M. Yoshikawa, T. Shirasawa, ALJ guidelines for practical applications of CFD to pedestrian wind environment around buildings, *J. Wind Eng. Ind. Aerod.* 96 (2008) 1749–1761, <https://doi.org/10.1016/j.jweia.2008.02.058>.
- [32] B. Blocken, *Computational Fluid Dynamics for urban physics: importance, scales, possibilities, limitations and ten tips and tricks towards accurate and reliable simulations*, *Build. Environ.* 91 (2015) 219–245, <https://doi.org/10.1016/j.buildenv.2015.02.015>.
- [33] Y. Abu-Zidan, P. Mendis, T. Gunawardena, Optimising the computational domain size in CFD simulations of tall buildings, *Heliyon* 7 (2021) e06723, <https://doi.org/10.1016/j.heliyon.2021.e06723>.
- [34] E. Diz-Mellado, V.P. López-Cabeza, C. Rivera-Gómez, C. Galán-Marín, Performance evaluation and users' perception of courtyards role in indoor areas of mediterranean social housing, *J. Environ. Manag.* 345 (2023) 118788, <https://doi.org/10.1016/j.jenvman.2023.118788>.
- [35] E. Diz-Mellado, V.P. López-Cabeza, C. Rivera-Gómez, C. Galán-Marín, Seasonal analysis of thermal comfort in Mediterranean social courtyards: a comparative study, *J. Build. Eng.* 78 (2023) 107756, <https://doi.org/10.1016/j.jobe.2023.107756>.
- [36] Seville, Spain Weather History, Weather Underground, (n.d.). <https://www.wunderground.com/history/daily/es/seville/LEZL/date/2023-7-17> (accessed August 7, 2023).
- [37] P.A. Vesilind, The Rosin-Rammler particle size distribution, *Resour. Recovery Conserv.* 5 (1980) 275–277, [https://doi.org/10.1016/0304-3967\(80\)90007-4](https://doi.org/10.1016/0304-3967(80)90007-4).
- [38] A.A. Bagasi, J.K. Calautit, Experimental field study of the integration of passive and evaporative cooling techniques with Mashrabiya in hot climates, *Energy Build.* 225 (2020) 110325, <https://doi.org/10.1016/j.enbuild.2020.110325>.